



HAL
open science

Connections and performances of Green's function methods for charged and neutral excitations

Enzo Monino, Pierre-François Loos

► **To cite this version:**

Enzo Monino, Pierre-François Loos. Connections and performances of Green's function methods for charged and neutral excitations. *The Journal of Chemical Physics*, 2023, 159 (3), pp.034105. 10.1063/5.0159853 . hal-04108975

HAL Id: hal-04108975

<https://hal.science/hal-04108975>

Submitted on 29 May 2023

HAL is a multi-disciplinary open access archive for the deposit and dissemination of scientific research documents, whether they are published or not. The documents may come from teaching and research institutions in France or abroad, or from public or private research centers.

L'archive ouverte pluridisciplinaire **HAL**, est destinée au dépôt et à la diffusion de documents scientifiques de niveau recherche, publiés ou non, émanant des établissements d'enseignement et de recherche français ou étrangers, des laboratoires publics ou privés.

Connections and performances of Green's function methods for charged and neutral excitations

Enzo Monino^{1, a)} and Pierre-François Loos^{1, b)}

Laboratoire de Chimie et Physique Quantiques (UMR 5626), Université de Toulouse, CNRS, UPS, France

In recent years, Green's function methods have garnered considerable interest due to their ability to target both charged and neutral excitations. Among them, the well-established *GW* approximation provides accurate ionization potentials and electron affinities and can be extended to neutral excitations using the Bethe-Salpeter equation (BSE) formalism. Here, we investigate the connections between various Green's function methods and evaluate their performance for charged and neutral excitations. Comparisons with other widely-known second-order wave function methods are also reported. Additionally, we calculate the singlet-triplet gap of cycl[3,3,3]azine, a model molecular emitter for thermally activated delayed fluorescence, which has the particularity of having an inverted gap thanks to a substantial contribution from the double excitations. We demonstrate that, within the *GW* approximation, a second-order BSE kernel with dynamical correction is required to predict this distinctive characteristic.

I. GREEN'S FUNCTION METHODS

Recent developments and investigations in Green's function approaches have generated significant interest within the electronic structure community,^{1–3} especially in quantum chemistry.^{4–7} The pillar of Green's function many-body perturbation theory is the one-body Green's function (or electron propagator).⁸ It has the ability to provide the charged excitations (*i.e.*, ionization potentials and electron affinities) of the system in a single calculation as measured in direct or inverse photoemission spectroscopy. This avoids using state-specific methods where one has to perform separate calculations on the neutral and ionized species.^{9–17}

Obviously, the exact one-body Green's function G is in general unknown but its mean-field Hartree-Fock (HF) version G_{HF} can be linked to the exact one, via a Dyson equation involving a key quantity known as the self-energy Σ , which includes correlation effects:

$$G(12) = G_{\text{HF}}(12) + \int G_{\text{HF}}(13)\Sigma(34)G(42)d3d4 \quad (1)$$

Here, $1 \equiv (\mathbf{x}_1, t_1)$ is a composite coordinate gathering spin-space and time variables.

The HF one-body Green's function is given by

$$G_{\text{HF}}(\mathbf{x}_1, \mathbf{x}_2; \omega) = \sum_i \frac{\psi_i(\mathbf{x}_1)\psi_i(\mathbf{x}_2)}{\omega - \epsilon_i^{\text{HF}} - i\eta} + \sum_a \frac{\psi_a(\mathbf{x}_1)\psi_a(\mathbf{x}_2)}{\omega - \epsilon_a^{\text{HF}} + i\eta} \quad (2)$$

where $\psi_p(\mathbf{x})$ is the p th HF spinorbital and ϵ_p^{HF} its corresponding energy, while η is a positive infinitesimal that we shall set to zero in the remaining of this paper. Throughout this article, we assume real orbitals and energies. The indices $p, q, r,$ and s are general spinorbitals, $i, j, k,$ and l denote occupied spinorbitals, $a, b, c,$ and d are vacant spinorbitals, while m and n label

single excitations/deexcitations and double electron attachments/detachments, respectively. Here, we systematically consider a HF starting point but the present analysis can be straightforwardly extended to a Kohn-Sham starting point.

Approximations to the self-energy, such as *GW*,^{5,18–21} are needed to solve the Dyson equation defined in Eq. (1). Even though the *GW* approximation has proven to produce accurate charged excitations in solids^{22–31} and molecules,^{6,7,32–65} it is not the only approximation to the self-energy. Indeed, other approximations exist such as the second-order Green's function (GF2),^{66–80} also known as second Born in the condensed matter community,^{3,81} the T -matrix^{82–96} (or Bethe-Goldstone approximation^{97–101}). Going beyond these approximations has been shown to be rather challenging.^{83,84,89,98,99,102–116} Here, for the sake of simplicity, we consider only one-shot schemes where one does not self-consistently update the self-energy,^{22,30,117–121} but the same analysis can be performed in the case of (partially) self-consistent schemes.^{26,46,122–130}

Another attractive point concerning Green's function-based techniques is the Bethe-Salpeter equation (BSE) formalism^{6,7,131,132} that allows access to the neutral (*i.e.*, optical) excitations of a given system. BSE relies on the two-body Green's function G_2 (or polarization propagator) via its link with the two-body correlation function

$$iL(12; 1'2') = -G_2(12; 1'2') + G(11')G(22') \quad (3)$$

that also satisfies a Dyson equation

$$L(12, 1'2') = L_0(12, 1'2') + \int L_0(14, 1'3)\Xi(35, 46)L(62, 52')d3d4d5d6 \quad (4)$$

with

$$iL_0(12; 1'2') = G(12')G(21') \quad (5)$$

and where

$$\Xi(13, 24) = i \frac{\delta \Sigma(12)}{\delta G(43)} \quad (6)$$

^{a)}Electronic mail: enzo.monino@irsamc.ups-tlse.fr

^{b)}Electronic mail: loos@irsamc.ups-tlse.fr

is the so-called BSE kernel. As we shall discuss later, like its time-dependent density-functional theory (TD-DFT) cousin,^{133–136} BSE can be written in the form of Casida-like equations.

Because the BSE kernel is the functional derivative of Σ with respect to G , one can readily see from Eq. (6) that Ξ strongly depends on the choice of approximate self-energy. The most popular BSE kernel is based on the GW approximation and leans on the dynamically-screened Coulomb potential W to provide rather accurate neutral excitations for molecular systems.¹³² However, one can also rely on kernels based on the T -matrix⁹⁶ or GF2.^{137–139}

Undoubtedly, the self-energy and kernel approximations discussed earlier possess inherent limitations, both stemming from their intrinsic nature and the typical methods employed to solve these equations, as well as potential additional approximations involved. For example, unphysical discontinuities in energy surfaces have been recently discovered and studied in the GW approximation^{54,140–143} but similar observations can be made with the other approximations. The issue can be traced down to the multiple solution character of the quasiparticle equation.¹⁴¹ This problem of discontinuities can be partially addressed by using linearization of the quasiparticle equation, but irregularities (or “bumps”) remain, for example, in potential energy surfaces.¹⁴¹ One can deal with this issue by using a static Coulomb-hole plus screened-exchange (COHSEX),^{26,105,142,144,145} by adopting a fully self-consistent scheme,^{143,146–155} or via regularization techniques.^{156,157}

Moreover, the BSE is considered, in general, within the so-called static approximation where the dynamical (*i.e.*, frequency-dependent) BSE kernel is approximated by its static limit. By doing so, the static BSE scheme,^{158–162} like the adiabatic approximation of TD-DFT,^{163–167} does not permit the description of double and higher excitations. The endeavor to go beyond the static approximation was first addressed by Strinati for core excitons in semiconductors.^{23,24,132,168} Then, using first-order perturbation theory, Rohlfing and co-workers have developed a way to take into account dynamical effects via the plasmon-pole approximation combined with the Tamm-Dancoff approximation (TDA).^{169–176} Recently, Loos and Blase¹⁶¹ proposed a dynamical scheme similar to Rohlfing’s that goes beyond the plasmon-pole approximation where the dynamical screening of the Coulomb interaction is computed exactly within the random-phase approximation (RPA).^{177–181}

Unfortunately, even though this dynamical scheme allows to dynamically correct the single excitations obtained from the static approach, it does not permit access to double excitations. A way to obtain these higher solutions is to resort to the spin-flip formalism where one considers a higher spin state as a reference.^{182,183} Note, however, that the spin-flip formalism does not give access to all double excitations and is hampered by spin contamination.^{184,185}

Recently, Backhouse and Booth have introduced an unfolding version of the non-linear GF2 equations which provides a linear eigenvalue problem of larger dimension⁷⁷ (see also Ref. 8). Bintrim and Berkelbach have extended it to the non-linear GW equations.¹⁸⁶ This linear eigenvalue problem allowed us to understand the role of intruder states in the origin of the energy surface discontinuities,¹⁵⁶ as well as the connections between Green’s function methods and coupled-cluster theory.^{187–189} More importantly, when combined with other computational techniques, the unfolding framework provides a way to significantly lower the computational scaling of these approaches.^{75–77,155,186} The same concept was also applied to the dynamical BSE eigenvalue problem built from the GW kernel in order to go beyond the static approximation.¹⁹⁰ This unfolding approach produces a linear eigenvalue problem in an expanded space of single and double excitations, hence direct access to doubly-excited states with, however, limited success in terms of accuracy.

In this work, we investigate both charged and neutral excitations in Secs. II and III, respectively. We begin by reviewing the equations associated with the GF2 (Sec. II B), GW (Sec. II C), and T -matrix (Sec. II D) self-energies in various forms. Subsequently, we present and study various static and dynamic BSE kernels based on the GF2 (Sec. III B), GW , (Secs. III C and III D), and T -matrix (Sec. III E) approximations, elucidating their interconnections and similarities with other theories. Computational details are provided in Sec. IV. In Sec. V A, we assess the accuracy of the three different self-energies in calculating the principal ionization potentials of a subset of atoms and molecules taken from the $GW100$ dataset.¹⁹¹ Section V B reports the computation of neutral excitations for another set of molecules using four different kernels within the static approximation. Additionally, we evaluate dynamical corrections through perturbation theory. Our analysis considers various types of excited states, predominantly valence and Rydberg states, and investigates the performance of these kernels based on the specific type of states. Finally, in Sec. V C, we compute, at various levels of theory, the gap between the first singlet and triplet excited states of cycl[3,3,3]azine, a model light-emitting diode (OLED) emitter for thermally activated delayed fluorescence (TADF), which has the particularity of having an inverted singlet-triplet gap. Our conclusions are presented in Sec. VI. Atomic units are consistently employed throughout.

II. CHARGED EXCITATIONS

A. Quasiparticle equation

Within the one-shot scheme, in order to obtain the quasiparticle energies and the corresponding satellites, one solve, for each spinorbital p and assuming real values of the frequency ω , the following (non-linear) quasiparti-

cle equation

$$\epsilon_p^{\text{HF}} + \Sigma_{pp}(\omega) - \omega = 0 \quad (7)$$

where $\Sigma_{pp}(\omega)$ is a diagonal element of the correlation part of the self-energy. Due to the fact that one is usually interested in the quasiparticle solution, Eq. (7) is often linearized around $\omega = \epsilon_p^{\text{HF}}$, *i.e.*,

$$\Sigma_{pp}(\omega) \approx \Sigma_{pp}(\epsilon_p^{\text{HF}}) + (\omega - \epsilon_p^{\text{HF}}) \left. \frac{\partial \Sigma_{pp}(\omega)}{\partial \omega} \right|_{\omega=\epsilon_p^{\text{HF}}} \quad (8)$$

which yields

$$\epsilon_p = \epsilon_p^{\text{HF}} + Z_p \Sigma_{pp}(\epsilon_p^{\text{HF}}) \quad (9)$$

where

$$Z_p = \left[1 - \left. \frac{\partial \Sigma_{pp}(\omega)}{\partial \omega} \right|_{\omega=\epsilon_p^{\text{HF}}} \right]^{-1} \quad (10)$$

is a renormalization factor ($0 \leq Z_p \leq 1$) which represents the spectral weight of the quasiparticle solution.

The non-linear quasiparticle equation (7) can be *exactly* transformed into a larger linear problem via the unfolding process mentioned earlier where the 2h1p and 2p1h sectors are unfolded from the 1h and 1p sectors.^{75-77,156,157,186,188,189,192} For each orbital p , this yields a linear eigenvalue problem of the form

$$\mathbf{H}_p \cdot \mathbf{c}_\nu = \epsilon_\nu \mathbf{c}_\nu \quad (11)$$

where ν runs over all solutions, quasiparticle and satellites, and with¹⁸⁹

$$\mathbf{H}_p = \begin{pmatrix} \epsilon_p^{\text{HF}} & \mathbf{V}_p^{2\text{h1p}} & \mathbf{V}_p^{2\text{p1h}} \\ \left(\mathbf{V}_p^{2\text{h1p}}\right)^\dagger & \mathbf{C}^{2\text{h1p}} & \mathbf{0} \\ \left(\mathbf{V}_p^{2\text{p1h}}\right)^\dagger & \mathbf{0} & \mathbf{C}^{2\text{p1h}} \end{pmatrix} \quad (12)$$

The diagonalization of \mathbf{H}_p is equivalent to solving the quasiparticle equation (7). This can be further illustrated by expanding the secular equation associated with Eq. (12)

$$\det[\mathbf{H}_p - \omega \mathbf{1}] = 0 \quad (13)$$

and comparing it with Eq. (7) by setting

$$\Sigma_{pp}(\omega) = \mathbf{V}_p^{2\text{h1p}} \cdot (\omega \mathbf{1} - \mathbf{C}^{2\text{h1p}})^{-1} \cdot \left(\mathbf{V}_p^{2\text{h1p}}\right)^\dagger + \mathbf{V}_p^{2\text{p1h}} \cdot (\omega \mathbf{1} - \mathbf{C}^{2\text{p1h}})^{-1} \cdot \left(\mathbf{V}_p^{2\text{p1h}}\right)^\dagger \quad (14)$$

where $\mathbf{1}$ is the identity matrix.

It can be readily seen from Eq. (12) that the hole (h) and particle (p) sectors are potentially coupled. This coupling, which is absent in coupled-cluster theory,^{187,188,193} is critical for generating effective higher-order diagrams in Green's function methods.⁸

In the present work, we look at various approximations for the dynamical self-energy $\Sigma_{pp}(\omega)$ and it obviously leads to different expressions for the blocks $\mathbf{C}^{2\text{h1p}}$, $\mathbf{C}^{2\text{p1h}}$, $\mathbf{V}_p^{2\text{h1p}}$, and $\mathbf{V}_p^{2\text{p1h}}$. In the following, for each approximation, we provide the expression for the self-energy and the different blocks.

B. GF2 self-energy

Within the GF2 approximation, one only takes into account the direct and exchange second-order diagrams,¹⁹⁴ and the self-energy is given by¹⁹⁵⁻¹⁹⁷

$$\Sigma^{\text{GF2}}(12) = G(12) \int v(13)G(34)G(43)v(42)d3d4 - \int G(13)v(14)G(34)G(42)v(32)d3d4 \quad (15)$$

where $v(12) = |\mathbf{r}_1 - \mathbf{r}_2|^{-1}$ is the bare Coulomb operator.

In the spinorbital basis, the self-energy is constituted by a hole and a particle term as follows

$$\Sigma_{pq}^{\text{GF2}}(\omega) = \frac{1}{2} \sum_{ija} \frac{\langle pa||ij\rangle \langle qa||ij\rangle}{\omega + \epsilon_a^{\text{HF}} - \epsilon_i^{\text{HF}} - \epsilon_j^{\text{HF}}} + \frac{1}{2} \sum_{iab} \frac{\langle pi||ab\rangle \langle qi||ab\rangle}{\omega + \epsilon_i^{\text{HF}} - \epsilon_a^{\text{HF}} - \epsilon_b^{\text{HF}}} \quad (16)$$

with $\langle pq||rs\rangle = \langle pq|rs\rangle - \langle pq|sr\rangle$ the antisymmetrized two-electron integrals written in Dirac's notation, *i.e.*,

$$\langle pq||rs\rangle = \iiint \psi_p(\mathbf{x}_1)\psi_q(\mathbf{x}_2)v(12)\psi_r(\mathbf{x}_1)\psi_s(\mathbf{x}_2)d\mathbf{x}_1d\mathbf{x}_2 \quad (17)$$

As mentioned above, one can rely on an equivalent linear eigenvalue problem [see Eq. (12)] where the diagonal blocks are given by^{8,77}

$$\mathbf{C}_{ija,klc}^{2\text{h1p}} = (-\epsilon_a^{\text{HF}} + \epsilon_i^{\text{HF}} + \epsilon_j^{\text{HF}})\delta_{ik}\delta_{jl}\delta_{ac} \quad (18a)$$

$$\mathbf{C}_{iab,kcd}^{2\text{p1h}} = (-\epsilon_i^{\text{HF}} + \epsilon_a^{\text{HF}} + \epsilon_b^{\text{HF}})\delta_{ik}\delta_{ac}\delta_{bd} \quad (18b)$$

and the corresponding coupling blocks read

$$\mathbf{V}_{p,klc}^{2\text{h1p}} = \frac{\langle pc||kl\rangle}{\sqrt{2}} \quad \mathbf{V}_{p,kcd}^{2\text{p1h}} = \frac{\langle pk||dc\rangle}{\sqrt{2}} \quad (19)$$

Using Eq. (14) we can see that one easily retrieves the self-energy expression in Eq. (16). As already discussed in the literature,^{8,75} it is worth mentioning that we recover the same secular equations as the second-order algebraic-diagrammatic construction [ADC(2)] treatment of the electron propagator in its Dyson form.^{8,198-201}

C. GW self-energy

GW is an approximation to Hedin's equations, a set of exact coupled integro-differential equations.¹⁴⁴ Diagrammatically, *GW* takes into account all the direct ring

diagrams via a resummation technique¹⁹⁴ and is adequate in the high-density regime where correlation is weak.^{202,203} Therefore, GW includes the second-order direct term contained in GF2 but lacks its second-order exchange counterpart. The GW approximation is a relatively low computational cost method^{147,204–209} that relies on the dynamically screened Coulomb potential W computed at the direct (*i.e.*, without exchange) particle-hole RPA (ph-RPA) level. In solids and large molecular systems, screening is usually significant, and the (frequency-dependent) screened Coulomb interaction is noticeably weaker than the (static) bare one.

The ph-RPA equations take the form of a non-Hermitian eigenvalue problem written in the basis of single excitations and deexcitations:

$$\begin{pmatrix} \mathbf{A}^{\text{ph}} & \mathbf{B}^{\text{ph}} \\ -\mathbf{B}^{\text{ph}} & -\mathbf{A}^{\text{ph}} \end{pmatrix} \cdot \begin{pmatrix} \mathbf{X}^{\text{ph}} & \mathbf{Y}^{\text{ph}} \\ \mathbf{Y}^{\text{ph}} & \mathbf{X}^{\text{ph}} \end{pmatrix} = \begin{pmatrix} \mathbf{X}^{\text{ph}} & \mathbf{Y}^{\text{ph}} \\ \mathbf{Y}^{\text{ph}} & \mathbf{X}^{\text{ph}} \end{pmatrix} \cdot \begin{pmatrix} \boldsymbol{\Omega}^{\text{ph}} & \mathbf{0} \\ \mathbf{0} & -\boldsymbol{\Omega}^{\text{ph}} \end{pmatrix} \quad (20)$$

with

$$A_{ia,jb}^{\text{ph}} = (\epsilon_a^{\text{HF}} - \epsilon_i^{\text{HF}})\delta_{ij}\delta_{ab} + \langle ib|aj \rangle \quad (21a)$$

$$B_{ia,jb}^{\text{ph}} = \langle ij|ab \rangle \quad (21b)$$

In the absence of instabilities, *i.e.*, when $\mathbf{A}^{\text{ph}} - \mathbf{B}^{\text{ph}}$ is positive definite, the ph-RPA problem reduces to a Hermitian problem of half the size. If one includes exchange in Eq. (21a) and (21b), one ends up with RPA with exchange (RPAX) which is equivalent to time-dependent HF (TDHF). Note that TDHF within the TDA, where one removes the coupling between excitations and deexcitations, *i.e.*, $\mathbf{B} = \mathbf{0}$, is equivalent to configuration interaction with singles (CIS).²¹⁰

Within the GW approximation, the self-energy is defined by the following simple expression:

$$\Sigma^{GW}(12) = iG(12)W(12) \quad (22)$$

which clearly justifies the name of this approximation. In the spinorbital basis, the self-energy reads

$$\Sigma_{pq}^{GW}(\omega) = \sum_{im} \frac{M_{pi,m}^{\text{ph}} M_{qi,m}^{\text{ph}}}{\omega - \epsilon_i^{\text{HF}} + \Omega_m^{\text{ph}}} + \sum_{am} \frac{M_{pa,m}^{\text{ph}} M_{qa,m}^{\text{ph}}}{\omega - \epsilon_a^{\text{HF}} - \Omega_m^{\text{ph}}} \quad (23)$$

where the screened two-electron integrals are given by

$$M_{pq,m}^{\text{ph}} = \sum_{ia} \langle pi|qa \rangle \left(\mathbf{X}^{\text{ph}} + \mathbf{Y}^{\text{ph}} \right)_{ia,m} \quad (24)$$

As shown by Bintrim and Berkelbach¹⁸⁶, and more recently by Tölle and Chan¹⁸⁹ (who have been able to eschew the use of the TDA), the blocks $\mathbf{C}^{2\text{h}1\text{p}}$ and $\mathbf{C}^{2\text{p}1\text{h}}$ defined in Eq. (12) are diagonal with elements

$$C_{im,im}^{2\text{h}1\text{p}} = \epsilon_i^{\text{HF}} - \Omega_m^{\text{ph}} \quad C_{am,am}^{2\text{p}1\text{h}} = \epsilon_a^{\text{HF}} + \Omega_m^{\text{ph}} \quad (25)$$

and the coupling blocks read

$$V_{p,im}^{2\text{h}1\text{p}} = M_{pi,m}^{\text{ph}} \quad V_{p,am}^{2\text{p}1\text{h}} = M_{pa,m}^{\text{ph}} \quad (26)$$

where $M_{pq,m}^{\text{ph}}$ are the screened integrals of Eq. (24). Using the expressions of the different blocks one can, via the inverse process, obtain the expression of the self-energy as described in Eq. (14) and recover Eq. (23).

Note that an attempt of decoupling the 2h1p and 2p1h spaces within GW , as it is done in non-Dyson ADC,²¹¹ has been made but with very mitigated results.¹⁸⁶

D. T -matrix self-energy

While GW depends on the dynamically screened Coulomb potential W , the T -matrix approximation relies on the so-called T -matrix, which, diagrammatically, corresponds to a resummation of a different class of diagrams known as ladder diagrams.¹⁹⁴ Unlike the two-point quantity W , the four-point T -matrix is spin-dependent, and mixes the singlet and triplet spin channels in the computation of the self-energy. The T -matrix approximation, which contains both second-order diagrams as well as additional higher-order ladder diagrams, is usually preferred to GW when the screening is weak or, in other words, in the low-density regime.

While W is computed using ph-RPA, the T -matrix is computed using the particle-particle (pp) RPA (pp-RPA) problem which is a non-Hermitian eigenvalue problem expressed in the basis of double electron attachments and double electron detachments:^{212–222}

$$\begin{pmatrix} \mathbf{C}^{\text{pp}} & \mathbf{B}^{\text{pp/hh}} \\ -\left(\mathbf{B}^{\text{pp/hh}}\right)^\dagger & -\mathbf{D}^{\text{hh}} \end{pmatrix} \cdot \begin{pmatrix} \mathbf{X}^{\text{pp}} & \mathbf{Y}^{\text{hh}} \\ \mathbf{Y}^{\text{pp}} & \mathbf{X}^{\text{hh}} \end{pmatrix} = \begin{pmatrix} \boldsymbol{\Omega}^{\text{pp}} & \mathbf{0} \\ \mathbf{0} & \boldsymbol{\Omega}^{\text{hh}} \end{pmatrix} \cdot \begin{pmatrix} \mathbf{X}^{\text{pp}} & \mathbf{Y}^{\text{hh}} \\ \mathbf{Y}^{\text{pp}} & \mathbf{X}^{\text{hh}} \end{pmatrix} \quad (27)$$

where

$$C_{ab,cd}^{\text{pp}} = (\epsilon_a^{\text{HF}} + \epsilon_b^{\text{HF}})\delta_{ac}\delta_{bd} + \langle ab|cd \rangle \quad (28a)$$

$$B_{ab,ij}^{\text{pp/hh}} = \langle ab||ij \rangle \quad (28b)$$

$$D_{ij,kl}^{\text{hh}} = -(\epsilon_i^{\text{HF}} + \epsilon_j^{\text{HF}})\delta_{ik}\delta_{jl} + \langle ij||kl \rangle \quad (28c)$$

with the following index restrictions $a < b$, $c < d$, $i < j$, and $k < l$.

Within the T -matrix approximation, the self-energy is

$$\Sigma^{GT}(12) = i \int G(43)T(13,24)d3d4 \quad (29)$$

and the elements of the self-energy in the spinorbital basis are explicitly given by^{89,94}

$$\Sigma_{pq}^{GT}(\omega) = \sum_{in} \frac{M_{pi,n}^{\text{pp}} M_{qi,n}^{\text{pp}}}{\omega + \epsilon_i^{\text{HF}} - \Omega_n^{\text{pp}}} + \sum_{an} \frac{M_{pa,n}^{\text{hh}} M_{qa,n}^{\text{hh}}}{\omega + \epsilon_a^{\text{HF}} - \Omega_n^{\text{hh}}} \quad (30)$$

where the pp and hh versions of the screened two-electron integrals read

$$M_{pq,n}^{\text{pp}} = \sum_{c<d} \langle pq||cd \rangle X_{cd,n}^{\text{pp}} + \sum_{k<l} \langle pq||kl \rangle Y_{kl,n}^{\text{pp}} \quad (31a)$$

$$M_{pq,n}^{\text{hh}} = \sum_{c<d} \langle pq||cd \rangle X_{cd,n}^{\text{hh}} + \sum_{k<l} \langle pq||kl \rangle Y_{kl,n}^{\text{hh}} \quad (31b)$$

Following the unfolding process of Bintrim and Berkelbach¹⁸⁶ together with the generalization of Tölle and Chan,¹⁸⁹ in the case of the T -matrix, we have the following diagonal elements for the blocks $C^{2\text{h}1\text{p}}$ and $C^{2\text{p}1\text{h}}$ of Eq. (12)

$$C_{an,an}^{2\text{h}1\text{p}} = -\epsilon_a^{\text{HF}} + \Omega_n^{\text{hh}} \quad C_{in,in}^{2\text{p}1\text{h}} = -\epsilon_i^{\text{HF}} + \Omega_n^{\text{pp}} \quad (32)$$

and the corresponding coupling blocks are

$$V_{p,an}^{2\text{h}1\text{p}} = M_{pa,n}^{\text{hh}} \quad V_{p,in}^{2\text{p}1\text{h}} = M_{pi,n}^{\text{pp}} \quad (33)$$

where the screened integrals are given by Eqs. (31a) and (31b).

III. NEUTRAL EXCITATIONS

A. Bethe-Salpeter equation

Within the BSE formalism, one must solve, in the general setting, a non-linear eigenvalue problem of the form

$$\begin{pmatrix} \mathbf{A}^{\text{BSE}}(\Omega_\nu^{\text{BSE}}) & \mathbf{B}^{\text{BSE}}(\Omega_\nu^{\text{BSE}}) \\ -\mathbf{B}^{\text{BSE}}(-\Omega_\nu^{\text{BSE}}) & -\mathbf{A}^{\text{BSE}}(-\Omega_\nu^{\text{BSE}}) \end{pmatrix} \cdot \begin{pmatrix} \mathbf{X}_\nu^{\text{BSE}} \\ \mathbf{Y}_\nu^{\text{BSE}} \end{pmatrix} = \Omega_\nu^{\text{BSE}} \begin{pmatrix} \mathbf{X}_\nu^{\text{BSE}} \\ \mathbf{Y}_\nu^{\text{BSE}} \end{pmatrix} \quad (34)$$

where the (anti)resonant block $\pm \mathbf{A}^{\text{BSE}}(\omega)$ and the coupling blocks $\pm \mathbf{B}^{\text{BSE}}(\omega)$ are dynamical quantities and the index ν runs over single, double, and potentially higher excitations. Of course, their expressions depend on the type of quasiparticles and the kernel that one considers but they have the following generic expressions

$$A_{ia,jb}^{\text{BSE}}(\omega) = A_{ia,jb} + \Xi_{ia,jb}(\omega) \quad (35a)$$

$$B_{ia,jb}^{\text{BSE}}(\omega) = B_{ia,jb} + \Xi_{ia,bj}(\omega) \quad (35b)$$

with the following static parts

$$A_{ia,jb} = (\epsilon_a - \epsilon_i) \delta_{ij} \delta_{ab} + \langle ib||aj \rangle \quad (36a)$$

$$B_{ia,jb} = \langle ij||ab \rangle \quad (36b)$$

where the ϵ_p 's are quasiparticle energies and $\Xi_{pq,rs}(\omega)$ is an element of the dynamical correlation kernel computed at a given level of theory. Note that, although these matrices are built in the single excitation and deexcitation manifolds, thanks to the frequency dependence of these quantities, one can potentially access higher excitations.

Again, one can enforce the TDA to obtain a simpler non-linear system

$$\mathbf{A}^{\text{BSE}}(\Omega_\nu^{\text{BSE}}) \cdot \mathbf{X}_\nu^{\text{BSE}} = \Omega_\nu^{\text{BSE}} \mathbf{X}_\nu^{\text{BSE}} \quad (37)$$

Below, we present three different ways of tackling the BSE problem.

First, one can enforce the so-called static approximation where one sets

$$A_{ia,jb}^{\text{BSE}} = A_{ia,jb} + \Xi_{ia,jb} \quad (38a)$$

$$B_{ia,jb}^{\text{BSE}} = B_{ia,jb} + \Xi_{ia,bj} \quad (38b)$$

to get

$$\begin{pmatrix} \mathbf{A}^{\text{BSE}} & \mathbf{B}^{\text{BSE}} \\ -\mathbf{B}^{\text{BSE}} & -\mathbf{A}^{\text{BSE}} \end{pmatrix} \cdot \begin{pmatrix} \mathbf{X}_m^{\text{BSE}} \\ \mathbf{Y}_m^{\text{BSE}} \end{pmatrix} = \Omega_m^{\text{BSE}} \begin{pmatrix} \mathbf{X}_m^{\text{BSE}} \\ \mathbf{Y}_m^{\text{BSE}} \end{pmatrix} \quad (39)$$

In this case, because of the frequency-independent nature of the static kernel's elements $\Xi_{pq,rs}$, one only accesses single excitations.

Second, one can go beyond the static approximation by using a renormalized first-order perturbative correction to the static BSE excitation energies. (We refer the interested reader to Ref. 161 for a detailed discussion. Here, we only provide the main equations.) This dynamical correction to the static BSE kernel (labeled dBSE in the following) allows us to recover additional relaxation effects coming from higher excitations.

The dBSE excitation energies are then obtained via

$$\Omega_m^{\text{dBSE}} = \Omega_m^{\text{BSE}} + \zeta_m \tilde{\Omega}_m^{\text{BSE}} \quad (40)$$

where the Ω_m^{BSE} 's are the static (zeroth-order) BSE excitation energies defined in Eq. (39) and

$$\tilde{\Omega}_m^{\text{BSE}} = (\mathbf{X}_m^{\text{BSE}})^\dagger \cdot \Delta \Xi(\Omega_m^{\text{BSE}}) \cdot \mathbf{X}_m^{\text{BSE}} \quad (41)$$

are first-order corrections obtained within the dynamical TDA (*i.e.*, as commonly done, only the resonant block is corrected for dynamical effects) with the renormalization factor

$$\zeta_m = \left[1 - (\mathbf{X}_m^{\text{BSE}})^\dagger \cdot \left. \frac{\partial \Delta \Xi(\omega)}{\partial \omega} \right|_{\omega=\Omega_m^{\text{BSE}}} \cdot \mathbf{X}_m^{\text{BSE}} \right]^{-1} \quad (42)$$

The generic expression for $\Delta \Xi(\omega)$ is

$$\Delta \Xi_{ia,jb}(\omega) = \tilde{\Xi}_{ia,jb}(\omega) - \Xi_{ia,jb} \quad (43)$$

where $\tilde{\Xi}_{ia,jb}(\omega)$ is an element of the so-called effective dynamical kernel. Unlike in the quasiparticle case (see Sec. II A), this renormalization factor ζ_m is not restricted between 0 and 1. However, it has been found to be close to unity in most cases which indicates the satisfactory convergence properties of the perturbative series.^{161,183}

Third, within the TDA, it is also possible to transform the non-linear eigenvalue problem (37) into a larger linear problem via an unfolding process where the 2h2p sector is unfolded from the 1h1p sector. The structure (and the dimension) of this matrix $\tilde{\mathbf{H}}$ depends on the nature and origin of the kernel. In the following, we present four different kernels and, for each of them, we provide the corresponding working equations.

B. Second-order GF2 kernel

We first discuss the BSE correlation kernel based on the GF2 self-energy considered in Eq. (15):

$$\Xi^{\text{GF2}}(35, 46) = i \frac{\delta \Sigma^{\text{GF2}}(34)}{\delta G(65)} \quad (44)$$

To avoid lengthy derivations and expressions, we refer the interested reader to the work of Zhang *et al.* (and particularly to the supplementary material) for the full derivation of the GF2 kernel.¹³⁷ Additional details and complements can be found in the work of Rebolini and Toulouse.^{138,223}

At the BSE@GF2 level, we have

$$A_{ia,jb}^{\text{GF2}}(\omega) = A_{ia,jb}^{\text{GF2}} + \Xi_{ia,jb}^{\text{GF2}}(\omega) \quad (45a)$$

$$B_{ia,jb}^{\text{GF2}}(\omega) = B_{ia,jb}^{\text{GF2}} + \Xi_{ia,bj}^{\text{GF2}}(\omega) \quad (45b)$$

with

$$A_{ia,jb}^{\text{GF2}} = (\epsilon_a^{\text{GF2}} - \epsilon_i^{\text{GF2}}) \delta_{ij} \delta_{ab} + \langle ib || aj \rangle \quad (46a)$$

$$B_{ia,jb}^{\text{GF2}} = \langle ij || ab \rangle \quad (46b)$$

and the elements of the second-order (with respect to the Coulomb interaction) static kernel for the (anti)resonant and coupling blocks are given by the following expression:

$$\begin{aligned} \Xi_{pq,rs}^{\text{GF2}} &= \sum_{kc} \frac{\langle rc || pk \rangle \langle kq || cs \rangle}{\epsilon_c^{\text{GF2}} - \epsilon_k^{\text{GF2}}} + \sum_{kc} \frac{\langle rk || pc \rangle \langle cq || ks \rangle}{\epsilon_c^{\text{GF2}} - \epsilon_k^{\text{GF2}}} \\ &+ \frac{1}{2} \sum_{kl} \frac{\langle qr || kl \rangle \langle lk || sp \rangle}{\epsilon_k^{\text{GF2}} + \epsilon_l^{\text{GF2}}} + \frac{1}{2} \sum_{cd} \frac{\langle qr || cd \rangle \langle dc || sp \rangle}{\epsilon_c^{\text{GF2}} + \epsilon_d^{\text{GF2}}} \end{aligned} \quad (47)$$

Going beyond the static approximation, the elements of the dynamical kernel for the resonant block are

$$\begin{aligned} \tilde{\Xi}_{ia,jb}^{\text{GF2}}(\omega) &= - \sum_{kc} \frac{\langle jc || ik \rangle \langle ka || cb \rangle}{\omega - (\epsilon_b^{\text{GF2}} + \epsilon_c^{\text{GF2}} - \epsilon_i^{\text{GF2}} - \epsilon_k^{\text{GF2}})} \\ &- \sum_{kc} \frac{\langle jk || ic \rangle \langle ca || kb \rangle}{\omega - (\epsilon_a^{\text{GF2}} + \epsilon_c^{\text{GF2}} - \epsilon_j^{\text{GF2}} - \epsilon_k^{\text{GF2}})} \\ &+ \frac{1}{2} \sum_{kl} \frac{\langle aj || kl \rangle \langle lk || bi \rangle}{\omega - (\epsilon_a^{\text{GF2}} + \epsilon_b^{\text{GF2}} - \epsilon_k^{\text{GF2}} - \epsilon_l^{\text{GF2}})} \\ &+ \frac{1}{2} \sum_{cd} \frac{\langle aj || cd \rangle \langle dc || bi \rangle}{\omega - (\epsilon_c^{\text{GF2}} + \epsilon_d^{\text{GF2}} - \epsilon_i^{\text{GF2}} - \epsilon_j^{\text{GF2}})} \end{aligned} \quad (48)$$

The first two terms in Eqs. (47) and (48) are ph and hp terms, while the third and fourth ones correspond to hh and pp terms, respectively.

Within the TDA, the unfolding process leads to the following linear eigenvalue problem

$$\tilde{\mathbf{H}}^{\text{GF2}} = \begin{pmatrix} \mathbf{A}^{\text{GF2}} & \mathbf{I} + \mathbf{K} & \mathbf{J} & \mathbf{K} \\ (\mathbf{J} + \mathbf{L})^\dagger & \mathbf{C}^{\text{GF2}} & \mathbf{0} & \mathbf{0} \\ \mathbf{K}^\dagger & \mathbf{0} & \mathbf{C}^{\text{GF2}} & \mathbf{0} \\ \mathbf{J}^\dagger & \mathbf{0} & \mathbf{0} & \mathbf{C}^{\text{GF2}} \end{pmatrix} \quad (49)$$

where, the block \mathbf{C}^{GF2} is diagonal with elements

$$C_{ijab,ijab}^{\text{GF2}} = \epsilon_a^{\text{GF2}} + \epsilon_b^{\text{GF2}} - \epsilon_i^{\text{GF2}} - \epsilon_j^{\text{GF2}} \quad (50)$$

while the various coupling terms read

$$I_{ia,klcd} = + \frac{\delta_{ac}}{\sqrt{2}} \langle di || kl \rangle \quad (51a)$$

$$J_{ia,klcd} = - \frac{\delta_{ad}}{\sqrt{2}} \langle ci || kl \rangle \quad (51b)$$

$$K_{ia,klcd} = + \frac{\delta_{il}}{\sqrt{2}} \langle dc || ak \rangle \quad (51c)$$

$$L_{ia,klcd} = - \frac{\delta_{ik}}{\sqrt{2}} \langle dc || al \rangle \quad (51d)$$

Note that, in this case, the unfolded matrix is non-Hermitian and contains three blocks of double excitations (*i.e.*, 2h2p configurations). Therefore, spurious (*i.e.*, non-physical) solutions are expected to appear due to the redundancy of the basis set.^{159,160,162} By downfolding the three subspaces of double excitations onto the space of single excitations, *i.e.*,

$$\begin{aligned} \tilde{\Xi}^{\text{GF2}}(\omega) &= (\mathbf{I} + \mathbf{K}) \cdot (\omega \mathbf{1} - \mathbf{C}^{\text{GF2}})^{-1} \cdot (\mathbf{J} + \mathbf{L})^\dagger \\ &+ \mathbf{J} \cdot (\omega \mathbf{1} - \mathbf{C}^{\text{GF2}})^{-1} \cdot \mathbf{K}^\dagger \\ &+ \mathbf{K} \cdot (\omega \mathbf{1} - \mathbf{C}^{\text{GF2}})^{-1} \cdot \mathbf{J}^\dagger \end{aligned} \quad (52)$$

one recovers exactly the dynamical kernel defined in Eq. (48).

Following Bintrimp and Berkelbach,¹⁹⁰ we attempt to symmetrize $\tilde{\mathbf{H}}^{\text{GF2}}$ and remove the redundant sets of 2h2p configurations by simply defining

$$\tilde{\mathbf{H}}^{\text{GF2}} = \begin{pmatrix} \mathbf{A}^{\text{HF}} & \mathbf{V} \\ \mathbf{V}^\dagger & \mathbf{C}^{\text{HF}} \end{pmatrix} \quad (53)$$

with $\mathbf{V} = (\mathbf{I} + \mathbf{J} + \mathbf{K} + \mathbf{L})/\sqrt{2}$, and

$$A_{ia,jb}^{\text{HF}} = (\epsilon_a^{\text{HF}} - \epsilon_i^{\text{HF}}) \delta_{ij} \delta_{ab} + \langle ib || aj \rangle \quad (54a)$$

$$C_{ijab,ijab}^{\text{HF}} = \epsilon_a^{\text{HF}} + \epsilon_b^{\text{HF}} - \epsilon_i^{\text{HF}} - \epsilon_j^{\text{HF}} \quad (54b)$$

In this case, we obtain the dynamical kernel

$$\tilde{\Xi}(\omega) = \mathbf{V} \cdot (\omega \mathbf{1} - \mathbf{C}^{\text{HF}})^{-1} \cdot \mathbf{V}^\dagger \quad (55)$$

with

$$\begin{aligned}
\bar{\Xi}_{ia,jb}^{\text{GF2}}(\omega) &= \frac{\delta_{ab}}{2} \sum_{klc} \frac{\langle kl||ic \rangle \langle kl||jc \rangle}{\omega - (\epsilon_a^{\text{HF}} + \epsilon_c^{\text{HF}} - \epsilon_k^{\text{HF}} - \epsilon_l^{\text{HF}})} \\
&+ \frac{\delta_{ij}}{2} \sum_{kcd} \frac{\langle ak||cd \rangle \langle bk||cd \rangle}{\omega - (\epsilon_c^{\text{HF}} + \epsilon_d^{\text{HF}} - \epsilon_k^{\text{HF}} - \epsilon_i^{\text{HF}})} \\
&- \sum_{kc} \frac{\langle jc||ik \rangle \langle ka||cb \rangle}{\omega - (\epsilon_b^{\text{HF}} + \epsilon_c^{\text{HF}} - \epsilon_k^{\text{HF}} - \epsilon_i^{\text{HF}})} \\
&- \sum_{kc} \frac{\langle jk||ic \rangle \langle ca||kb \rangle}{\omega - (\epsilon_a^{\text{HF}} + \epsilon_c^{\text{HF}} - \epsilon_k^{\text{HF}} - \epsilon_j^{\text{HF}})} \\
&+ \frac{1}{2} \sum_{kl} \frac{\langle aj||kl \rangle \langle lk||bi \rangle}{\omega - (\epsilon_a^{\text{HF}} + \epsilon_b^{\text{HF}} - \epsilon_k^{\text{HF}} - \epsilon_l^{\text{HF}})} \\
&+ \frac{1}{2} \sum_{cd} \frac{\langle aj||cd \rangle \langle dc||bi \rangle}{\omega - (\epsilon_c^{\text{HF}} + \epsilon_d^{\text{HF}} - \epsilon_i^{\text{HF}} - \epsilon_j^{\text{HF}})}
\end{aligned} \tag{56}$$

where one can see that we recover the four terms of the

original dynamical kernel (48) with two additional self-energy terms that correspond to partial renormalization of the particle and hole sectors of the self-energy (forward time-ordered diagrams). Therefore, in order to avoid double counting, one must use HF orbital energies instead of GF2 quasiparticle energies in Eq. (53). However, the particle (hole) propagator is only renormalized by the 2p1h (2h1p) configurations and not the 2h1p (2p1h) configurations.

The expression (56) has a strong connection with the ADC(2) method for the polarization propagator (*i.e.*, for neutral excitations).^{198,201,224-226} Indeed, the blocks \mathbf{C}^{HF} and \mathbf{V} in ADC(2) have identical expressions. However, in ADC(2), the 1h1p block has three additional second-order static terms. By replacing \mathbf{A}^{HF} by $\mathbf{A}^{\text{HF}} + \bar{\mathbf{A}}^{\text{GF2}}$ in Eq. (53) with

$$\begin{aligned}
\bar{A}_{ia,jb}^{\text{GF2}} &= \frac{\delta_{ij}}{4} \sum_{klc} \left[\frac{\langle ac||kl \rangle \langle kl||bc \rangle}{\epsilon_a^{\text{HF}} - \epsilon_k^{\text{HF}} + \epsilon_c^{\text{HF}} - \epsilon_l^{\text{HF}}} + \frac{\langle ac||kl \rangle \langle kl||bc \rangle}{\epsilon_b^{\text{HF}} - \epsilon_k^{\text{HF}} + \epsilon_c^{\text{HF}} - \epsilon_l^{\text{HF}}} \right] \\
&+ \frac{\delta_{ab}}{4} \sum_{kcd} \left[\frac{\langle cd||ik \rangle \langle jk||cd \rangle}{\epsilon_c^{\text{HF}} - \epsilon_i^{\text{HF}} + \epsilon_d^{\text{HF}} - \epsilon_k^{\text{HF}}} + \frac{\langle cd||ik \rangle \langle jk||cd \rangle}{\epsilon_c^{\text{HF}} - \epsilon_j^{\text{HF}} + \epsilon_d^{\text{HF}} - \epsilon_k^{\text{HF}}} \right] \\
&- \frac{1}{2} \sum_{kc} \left[\frac{\langle ac||ik \rangle \langle jk||bc \rangle}{\epsilon_a^{\text{HF}} - \epsilon_i^{\text{HF}} + \epsilon_c^{\text{HF}} - \epsilon_k^{\text{HF}}} + \frac{\langle ac||ik \rangle \langle jk||bc \rangle}{\epsilon_b^{\text{HF}} - \epsilon_j^{\text{HF}} + \epsilon_c^{\text{HF}} - \epsilon_k^{\text{HF}}} \right]
\end{aligned} \tag{57}$$

one ends up with exactly the ADC(2) secular equations. Although static, the first two terms are particularly crucial as they complete the renormalization of the HF orbital energies via the introduction of the missing backward time-ordered diagrams.

C. First-order GW kernel

Within the GW approximation, using the self-energy defined in Eq. (22), the BSE kernel reads^{19,227-229}

$$\begin{aligned}
\frac{\delta \Sigma^{GW}(34)}{\delta G(65)} &= - \frac{\delta(G(34)W(34))}{\delta G(65)} \\
&= -W(34) \frac{\delta G(34)}{\delta G(65)} - G(34) \frac{\delta W(34)}{\delta G(65)} \\
&= \Xi^{GW}(35,46) + \Theta^{GW}(35,46)
\end{aligned} \tag{58}$$

and it is common practice to neglect Θ^{GW} .^{23,24,132,168,230} (We shall come back to this point later on.) Thus, one gets the following static kernel elements¹³²

$$\Xi_{pq,rs}^{GW} = 2 \sum_m \frac{M_{pr,m}^{\text{ph}} M_{qs,m}^{\text{ph}}}{\Omega_m^{\text{ph}}} \tag{59}$$

As for the GF2 case, it is possible to go beyond the static approximation by taking into account the dynamical structure of W , that is,¹⁸³

$$\begin{aligned}
\bar{\Xi}_{ia,jb}^{GW}(\omega) &= - \sum_m \frac{M_{ij,m}^{\text{ph}} M_{ab,m}^{\text{ph}}}{\omega - (\epsilon_b^{GW} - \epsilon_i^{GW} + \Omega_m^{\text{ph}})} \\
&- \sum_m \frac{M_{ij,m}^{\text{ph}} M_{ab,m}^{\text{ph}}}{\omega - (\epsilon_a^{GW} - \epsilon_j^{GW} + \Omega_m^{\text{ph}})}
\end{aligned} \tag{60}$$

By removing the screening effects from GW , *i.e.*, by performing the following substitutions, $\Omega_m^{\text{ph}} \rightarrow \epsilon_a^{\text{HF}} - \epsilon_i^{\text{HF}}$ and $M_{pq,m}^{\text{ph}} \rightarrow \langle pi|qa \rangle$, one recovers the two ph terms of Eq. (48), without, of course, the exchange part.

As shown in Ref. 190, at the BSE@ GW level, the up-folding process yields

$$\tilde{\mathbf{H}}^{GW} = \begin{pmatrix} \mathbf{A}^{GW} & \mathbf{J}^{\text{ph}} & \mathbf{K}^{\text{ph}} \\ (\mathbf{K}^{\text{ph}})^{\dagger} & \mathbf{C}^{GW} & \mathbf{0} \\ (\mathbf{J}^{\text{ph}})^{\dagger} & \mathbf{0} & \mathbf{C}^{GW} \end{pmatrix} \tag{61}$$

with the usual static expression for the 1h1p part

$$A_{ia,jb}^{GW} = (\epsilon_a^{GW} - \epsilon_i^{GW}) \delta_{ij} \delta_{ab} + \langle ib||aj \rangle \tag{62}$$

a diagonal 2h2p block with elements

$$C_{iam,iam}^{GW} = \Omega_m^{\text{ph}} + \epsilon_a^{GW} - \epsilon_i^{GW} \quad (63)$$

and coupling blocks that read

$$J_{ia,kcm}^{\text{ph}} = -\delta_{ac} M_{ik,m}^{\text{ph}} \quad (64a)$$

$$K_{ia,kcm}^{\text{ph}} = +\delta_{ik} M_{ac,m}^{\text{ph}} \quad (64b)$$

Again, $\tilde{\mathbf{H}}^{GW}$ is a non-Hermitian matrix with two sets of double excitations. By downfolding we get

$$\begin{aligned} \tilde{\Xi}^{GW}(\omega) &= \mathbf{J}^{\text{ph}} \cdot (\omega \mathbf{1} - \mathbf{C}^{GW})^{-1} \cdot (\mathbf{K}^{\text{ph}})^\dagger \\ &+ \mathbf{K}^{\text{ph}} \cdot (\omega \mathbf{1} - \mathbf{C}^{GW})^{-1} \cdot (\mathbf{J}^{\text{ph}})^\dagger \end{aligned} \quad (65)$$

which gives us back the dynamical kernel (60). As proposed by Bintrim and Berkelbach,¹⁹⁰ one can also symmetrize $\tilde{\mathbf{H}}^{GW}$ and remove the additional 2h2p block by defining

$$\bar{\mathbf{H}}^{GW} = \begin{pmatrix} \mathbf{A}^{\text{HF}} + \bar{\mathbf{A}}^{GW} & \mathbf{J}^{\text{ph}} + \mathbf{K}^{\text{ph}} \\ (\mathbf{J}^{\text{ph}} + \mathbf{K}^{\text{ph}})^\dagger & \bar{\mathbf{C}}^{GW} \end{pmatrix} \quad (66)$$

with

$$\bar{C}_{iam,iam}^{GW} = \Omega_m^{\text{ph}} + \epsilon_a^{\text{HF}} - \epsilon_i^{\text{HF}} \quad (67)$$

but, again, the resulting dynamical kernel

$$\bar{\Xi}^{GW}(\omega) = (\mathbf{J}^{\text{ph}} + \mathbf{K}^{\text{ph}}) \cdot (\omega \mathbf{1} - \bar{\mathbf{C}}^{GW})^{-1} \cdot (\mathbf{J}^{\text{ph}} + \mathbf{K}^{\text{ph}})^\dagger \quad (68)$$

contains additional self-energy terms:

$$\begin{aligned} \bar{\Xi}_{ia,jb}^{GW}(\omega) &= \delta_{ab} \sum_{km} \frac{M_{ik,m}^{\text{ph}} M_{jk,m}^{\text{ph}}}{\omega - (\epsilon_a^{\text{HF}} - \epsilon_k^{\text{HF}} + \Omega_m^{\text{ph}})} \\ &+ \delta_{ij} \sum_{cm} \frac{M_{ac,m}^{\text{ph}} M_{bc,m}^{\text{ph}}}{\omega - (\epsilon_c^{\text{HF}} - \epsilon_i^{\text{HF}} + \Omega_m^{\text{ph}})} \\ &- \sum_m \frac{M_{ij,m}^{\text{ph}} M_{ab,m}^{\text{ph}}}{\omega - (\epsilon_b^{\text{HF}} - \epsilon_i^{\text{HF}} + \Omega_m^{\text{ph}})} \\ &- \sum_m \frac{M_{ij,m}^{\text{ph}} M_{ab,m}^{\text{ph}}}{\omega - (\epsilon_a^{\text{HF}} - \epsilon_j^{\text{HF}} + \Omega_m^{\text{ph}})} \end{aligned} \quad (69)$$

It has been found to severely affect the excitation energies due to the lack of backward time-ordered diagrams in the self-energy.¹⁹⁰ Hence, inspired by the ADC(2) expression, one could consider adding the missing self-energy terms (which correspond to the inclusion of the backward time-ordered diagrams) by defining the elements of $\bar{\mathbf{A}}^{GW}$ in

Eq. (66) as

$$\begin{aligned} \bar{A}_{ia,jb}^{GW} &= \frac{\delta_{ij}}{2} \sum_{km} \left[\frac{M_{ak,m}^{\text{ph}} M_{bk,m}^{\text{ph}}}{\epsilon_a^{\text{HF}} - \epsilon_k^{\text{HF}} + \Omega_m^{\text{ph}}} + \frac{M_{ak,m}^{\text{ph}} M_{bk,m}^{\text{ph}}}{\epsilon_b^{\text{HF}} - \epsilon_k^{\text{HF}} + \Omega_m^{\text{ph}}} \right] \\ &- \frac{\delta_{ab}}{2} \sum_{cm} \left[\frac{M_{ic,m}^{\text{ph}} M_{jc,m}^{\text{ph}}}{\epsilon_i^{\text{HF}} - \epsilon_c^{\text{HF}} - \Omega_m^{\text{ph}}} + \frac{M_{ic,m}^{\text{ph}} M_{jc,m}^{\text{ph}}}{\epsilon_j^{\text{HF}} - \epsilon_c^{\text{HF}} - \Omega_m^{\text{ph}}} \right] \end{aligned} \quad (70)$$

One can then solely rely on HF orbital energies in the previous expressions, instead of the GW quasiparticles.¹⁹⁰ The study of the performance of this new scheme is left for future work.

D. Second-order GW kernel

As mentioned above, it is customary to neglect the functional derivative $\delta W/\delta G$ in the expression of the GW kernel [see Eq. (58)]. However, a second-order GW kernel, Θ^{GW} , that takes into account this additional term has been recently derived by Yamada *et al.*²³¹ and tested on the Thiel benchmark set²³²⁻²³⁵ within the plasmon-pole approximation. In the following, we refer to this scheme as BSE2@ GW .

The second-order GW kernel is naturally divided into two terms as follows:

$$\begin{aligned} \Theta^{GW}(35, 46) &= iG(35)G(64)W(34)W(56) \\ &+ iG(35)G(64)W(36)W(54) \end{aligned} \quad (71)$$

Contrary to Ξ^{GW} which corresponds to the screening of the exchange term, the two additional second-order terms included in Θ^{GW} screen the direct term. As a consequence, BSE2@ GW only alters the excitation energies of the singlet excited states, while triplet states remain unaffected by this second-order correction.

In the spinorbital basis, we obtain the following static kernel elements:

$$\begin{aligned} \Theta_{pq,rs}^{GW} &= \sum_{kc} \frac{W_{rk,pc} W_{qc,sk}}{\epsilon_c^{GW} - \epsilon_k^{GW}} + \sum_{kc} \frac{W_{rc,pk} W_{qk,sc}}{\epsilon_c^{GW} - \epsilon_k^{GW}} \\ &+ \sum_{kl} \frac{W_{qr,kl} W_{kl,ps}}{\epsilon_k^{GW} + \epsilon_l^{GW}} - \sum_{cd} \frac{W_{qr,cd} W_{cd,ps}}{\epsilon_c^{GW} + \epsilon_d^{GW}} \end{aligned} \quad (72)$$

where

$$W_{pq,rs} = -\langle pq|rs \rangle + \Xi_{pq,rs}^{GW} \quad (73)$$

are the elements of the dynamically-screened Coulomb potential in its static limit, while the elements of the

dynamical kernel for the resonant block are²³¹

$$\begin{aligned}\tilde{\Theta}_{ia,jb}^{GW}(\omega) = & - \sum_{kc} \frac{W_{ac,bk}W_{jk,ic}}{\omega - (\epsilon_a^{GW} + \epsilon_c^{GW} - \epsilon_k^{GW} - \epsilon_j^{GW})} \\ & - \sum_{kc} \frac{W_{ak,bc}W_{ki,cj}}{\omega - (\epsilon_c^{GW} + \epsilon_b^{GW} - \epsilon_i^{GW} - \epsilon_k^{GW})} \\ & + \sum_{cd} \frac{W_{aj,cd}W_{cd,ib}}{\omega - (\epsilon_c^{GW} + \epsilon_d^{GW} - \epsilon_j^{GW} - \epsilon_i^{GW})} \\ & + \sum_{kl} \frac{W_{aj,kl}W_{kl,ib}}{\omega - (\epsilon_a^{GW} + \epsilon_b^{GW} - \epsilon_k^{GW} - \epsilon_l^{GW})}\end{aligned}\quad (74)$$

where one readily sees that hp, ph, pp, and hh contributions are included at the BSE2@GW level. As for the GF2 kernel (see Sec. III B), one can easily derive an upfolded version of this second-order kernel.

E. First-order T -matrix kernel

Another possible BSE kernel can be constructed using the T -matrix self-energy [see Eq. (29)]. A detailed study of this kernel is performed in Ref. 96. Following a similar derivation as the GW kernel, one gets at the BSE@ GT level

$$\begin{aligned}\Xi^{GT}(35, 46) &= i \frac{\delta \Sigma^{GT}(34)}{\delta G(65)} = - \frac{\delta(G(87)T(37, 48))}{\delta G(65)} \\ &= -T(37, 48) \frac{\delta G(87)}{\delta G(65)} - G(87) \frac{\delta T(37, 48)}{\delta G(65)} \\ &= -T(35, 46)\end{aligned}\quad (75)$$

where again we neglect the functional derivative $\delta T/\delta G$. (To be best of our knowledge, a second-order expression of the T -matrix kernel has not yet been derived.)

The elements of the static T -matrix kernel are given by⁹⁴

$$\Xi_{pq,rs}^{GT} = - \sum_n \frac{M_{pq,n}^{pp} M_{rs,n}^{pp}}{\Omega_n^{pp}} + \sum_n \frac{M_{pq,n}^{hh} M_{rs,n}^{hh}}{\Omega_n^{hh}} \quad (76)$$

where the expressions for the screened integrals have already been established in Sec. II D.

Going beyond the static approximation, one gets the dynamical T -matrix kernel⁹⁶

$$\begin{aligned}\tilde{\Xi}_{ia,jb}^{GT}(\omega) &= \sum_n \frac{M_{aj,n}^{pp} M_{bi,n}^{pp}}{\omega - (\Omega_n^{pp} - \epsilon_i^{GT} - \epsilon_j^{GT})} \\ &+ \sum_n \frac{M_{aj,n}^{hh} M_{bi,n}^{hh}}{\omega - (\epsilon_a^{GT} + \epsilon_b^{GT} - \Omega_n^{hh})}\end{aligned}\quad (77)$$

It is interesting to note that, by removing the resummation effect of the T -matrix, *i.e.*, by performing the following substitutions, $\Omega_n^{pp} \rightarrow \epsilon_a^{HF} + \epsilon_b^{HF}$, $\Omega_n^{hh} \rightarrow \epsilon_i^{HF} + \epsilon_j^{HF}$,

$M_{pq,m}^{pp} \rightarrow \langle pq||cd \rangle$, and $M_{pq,m}^{hh} \rightarrow \langle pq||ij \rangle$, one recovers both the direct and exchange parts of the pp and hh terms from Eq. (48).

The upfolding process gives us

$$\tilde{\mathbf{H}}^{GT} = \begin{pmatrix} \mathbf{A}^{GT} & \mathbf{K}^{pp} & \mathbf{I}^{hh} \\ (\mathbf{L}^{pp})^\dagger & \mathbf{C}^{pp} & \mathbf{0} \\ (\mathbf{J}^{hh})^\dagger & \mathbf{0} & \mathbf{C}^{hh} \end{pmatrix} \quad (78)$$

with

$$A_{ia,jb}^{GT} = (\epsilon_a^{GT} - \epsilon_i^{GT})\delta_{ij}\delta_{ab} + \langle ib||aj \rangle \quad (79)$$

and the following expressions for the diagonal blocks \mathbf{C}^{pp} and \mathbf{C}^{hh}

$$C_{ijn,ijn}^{pp} = \Omega_n^{pp} - \epsilon_i^{GT} - \epsilon_j^{GT} \quad (80a)$$

$$C_{abn,abn}^{hh} = \epsilon_a^{GT} + \epsilon_b^{GT} - \Omega_n^{hh} \quad (80b)$$

while the coupling blocks read

$$I_{ia,cdn}^{hh} = \delta_{ac}M_{di,n}^{hh} \quad J_{ia,cdn}^{hh} = \delta_{ad}M_{ci,n}^{hh} \quad (81a)$$

$$K_{ia,klm}^{pp} = \delta_{il}M_{ak,n}^{pp} \quad L_{ia,klm}^{pp} = \delta_{ik}M_{al,n}^{pp} \quad (81b)$$

By downfolding Eq. (78), we obtain

$$\begin{aligned}\tilde{\Xi}^{GT}(\omega) &= \mathbf{K}^{pp} \cdot (\omega\mathbf{1} - \mathbf{C}^{pp})^{-1} \cdot (\mathbf{L}^{pp})^\dagger \\ &+ \mathbf{I}^{hh} \cdot (\omega\mathbf{1} - \mathbf{C}^{hh})^{-1} \cdot (\mathbf{J}^{hh})^\dagger\end{aligned}\quad (82)$$

which gives back the dynamical kernel (77). Symmetrizing Eq. (78) has been revealed to be challenging, and we have not found any satisfying form.

IV. COMPUTATIONAL DETAILS

All systems investigated in this study possess a closed-shell singlet ground state, and thus we employ the restricted formalism exclusively. As mentioned earlier, we initiate all calculations from HF orbitals and energies. We focus on two sets of atoms and molecules: one set pertains to charged excitations, where we solely consider the principal ionization potentials (IPs), while the other set concerns neutral excitations, where we compute singlet and triplet vertical excitation energies. In all calculations, the positive infinitesimal η is set to zero.

The first set comprises 20 atoms and molecules from the $GW100$ test set,¹⁹¹ denoted as $GW20$, previously explored in Refs. 236 and 237. We adopt the geometries for the $GW20$ set from Ref. 191. Calculations of IPs are performed using three different schemes: GF2, GW , and GT . All occupied and virtual orbitals are corrected. For each scheme, we compute the linearized solution of the quasiparticle equation by solving Eq. (9) and the dynamical solution by employing Newton's method starting from the linearized solution. The results presented in the [supplementary material](#) indicate that the

linearization procedure has minimal impact on the GW and GT quasiparticles energies, while it improves the accuracy of GF2. Consequently, all quasiparticle energies are obtained via linearization of quasiparticle equation [see Eq. (9)]. It is important to note that the GW and GT calculations are carried out without the TDA for the calculation of W and T , respectively. As reference data, we rely on CCSD(T) IPs computed in the same basis.

The second set comprises 7 molecules as considered in Ref. 161. The corresponding geometries are extracted from the same work. Singlet and triplet transition energies are computed using the aug-cc-pVTZ basis via BSE utilizing the quasiparticle energies and kernels from the three different approximations under consideration (GF2, GW , and GT). For each scheme (BSE@GF2, BSE@ GW , BSE2@ GW , and BSE@ GT), we also incorporate their respective dynamical corrections, named dBSE@GF2, dBSE@ GW , dBSE2@ GW , and dBSE@ GT . To facilitate comparison, we also perform TDHF and CIS calculations. Our results are benchmarked against the theoretical best estimates (TBEs) from Ref. 161, from which we also extract transition energies computed using various second-order methods: CIS(D),^{238,239} ADC(2),^{201,240} CC2,²⁴¹ and EOM-CCSD.^{242,243}

Various statistical quantities with respect to the reference values [CCSD(T) for IPs and TBEs for transition energies] are reported: mean absolute error (MAE), mean signed error (MSE), root-mean-square error (RMSE), and maximum error (Max). All static and dynamic BSE calculations, as well as CIS and TDHF calculations, are performed using the freely available software QUACK, which can be found on GITHUB.²⁴⁴

V. RESULTS AND DISCUSSION

A. Ionization potentials

The IPs of the $GW20$ set using the different approximations of the self-energy are reported in Table I, where we also report the HF values. It clearly shows the superiority of the GW approximation for the calculation of IPs compared to the GF2 approximation. Indeed, we can see that the different statistical errors associated with GW (MAE and MSE of 0.28 eV and 0.23 eV, respectively) are much smaller than the ones of GF2 (MAE and MSE of 0.56 eV and -0.55 eV, respectively). For example, we have a maximum error of 1.60 eV for GF2 whereas GW has a maximum error of 0.85 eV. We can note that the GT approximation (MAE and MSE of 0.26 eV and -0.18 eV, respectively) presents a similar MAE and maximum error as GW , while its MSE has also a similar magnitude but opposite sign. An analogous conclusion was reached by Zhang and coworkers for larger systems.⁹⁴

TABLE I. Principal IPs (in eV) of the $GW20$ set computed with various approximations using the cc-pVTZ basis.

Mol.	HF	GF2	GW	GT	Δ CCSD(T)
He	24.97	24.54	24.58	24.77	24.53
Ne	23.01	20.13	21.40	21.02	21.30
H ₂	16.17	16.31	16.49	16.26	16.40
Li ₂	4.95	5.19	5.35	5.04	5.23
LiH	8.20	7.99	8.16	8.14	7.99
HF	17.53	14.72	16.18	15.63	15.98
Ar	16.06	15.39	15.70	15.49	15.53
H ₂ O	13.75	11.52	12.81	12.24	12.53
LiF	12.92	9.81	11.38	10.95	11.39
HCl	12.95	12.40	12.75	12.48	12.59
BeO	10.50	8.38	9.78	9.21	9.98
CO	15.35	14.17	15.03	14.44	14.21
N ₂	17.23	15.09	17.09	15.70	15.49
CH ₄	14.84	14.11	14.75	14.28	14.38
BH ₃	13.56	13.25	13.65	13.30	13.28
NH ₃	11.61	10.18	11.15	10.62	10.78
BF	11.00	11.02	11.29	10.92	11.09
BN	11.52	10.99	11.70	11.12	11.99
SH ₂	10.46	10.15	10.46	10.15	10.32
F ₂	18.09	14.26	16.31	15.38	15.68
MAE	0.81	0.56	0.28	0.26	
MSE	0.70	-0.55	0.23	-0.18	
RMSE	1.04	0.80	0.36	0.34	
Max	2.41	1.60	0.85	0.87	

B. Vertical transition energies

The results of our calculations for vertical transition energies using the aug-cc-pVTZ basis set are summarized in Tables II and III for the singlet and triplet excited states, respectively. They also report separate statistical errors for different classes of singlet and triplet excitations: valence (Val.) and Rydberg (Ryd.) excited states.

As expected, both CIS and TDHF exhibit large statistical errors compared to the TBEs. It is well known that TDHF provides a poor description of triplet excitations, often leading to triplet instabilities.^{210,245} One notices that TDHF is particularly bad at valence excitations. On the other hand, CIS provides a more balanced description of singlets and triplets, thanks to error cancellation.

In the [supplementary material](#), we report additional TDHF calculations using the GF2, GW , and GT quasiparticles (without their corresponding kernel) instead of HF orbital energies. These calculations, referred to as TDHF@GF2, TDHF@ GW , and TDHF@ GT , allow us to observe the effects of different kernels and quasiparticles on the excitation energies. We find that the sole introduction of quasiparticle energies does not improve the description of singlet excitations. It should be noted that these calculations for triplet excitations resulted in instabilities and are not shown.

The inclusion of the corresponding BSE kernel significantly improves the description of both singlet and triplet

TABLE II. Singlet excitation energies (in eV) of various molecules computed using the aug-cc-pVTZ basis set at different levels of theory. The dynamically-corrected BSE transition energies (dBSE) are reported in parentheses. CT stands for charge transfer. The statistical descriptors associated with the errors with respect to the reference values are also reported for the entire dataset and separately for valence (Val.) and Rydberg (Ryd.) excited states.

Mol.	Nature	CIS	TDHF	BSE@GF2	BSE@GW	BSE2@GW	BSE@GT	CIS(D)	ADC(2)	CC2	CCSD	TBE
HCl	CT	8.32	8.27	8.17 (7.99)	8.30 (8.19)	8.48 (8.36)	7.56 (7.52)	6.07	7.97	7.96	7.91	7.84
H ₂ O	Ryd.	8.69	8.64	7.13 (7.01)	8.09 (8.01)	8.24 (8.14)	7.12 (7.08)	7.62	7.18	7.23	7.60	7.17
	Ryd.	10.36	10.31	8.71 (8.66)	9.80 (9.72)	9.91 (9.84)	8.88 (8.84)	9.41	8.84	8.89	9.36	8.92
N ₂	Ryd.	10.96	10.93	9.49 (9.36)	10.42 (10.35)	10.53 (10.45)	9.55 (9.51)	9.99	9.52	9.58	9.96	9.52
	Val.	9.95	9.70	9.83 (9.28)	10.42 (9.99)	11.28 (10.74)	7.89 (7.78)	9.66	9.48	9.44	9.41	9.34
	Val.	8.43	7.86	10.72 (9.69)	10.11 (9.66)	11.35 (10.70)	8.18 (8.02)	10.31	10.26	10.32	10.00	9.88
	Val.	8.98	8.68	11.28 (10.34)	10.75 (10.33)	11.45 (10.86)	8.47 (8.36)	10.85	10.79	10.86	10.44	10.29
	Ryd.	14.48	14.46	12.30 (12.29)	13.60 (13.57)	13.61 (13.57)	12.71 (12.68)	13.67	12.99	12.83	13.15	12.98
	Ryd.	14.95	14.87	14.19 (14.07)	13.98 (13.94)	14.08 (14.03)	13.69 (13.66)	13.64	13.32	13.15	13.43	13.03
CO	Ryd.	14.42	13.98	12.84 (12.84)	13.98 (13.91)	14.13 (14.08)	13.16 (13.11)	13.75	13.07	12.89	13.26	13.09
	Ryd.	13.56	13.54	12.99 (12.96)	14.24 (14.21)	14.30 (14.27)	13.54 (13.47)	14.52	14.00	13.96	13.67	13.46
	Val.	9.00	8.72	9.40 (8.84)	9.54 (9.20)	10.15 (9.74)	7.63 (7.53)	8.78	8.69	8.64	8.59	8.49
	Val.	9.61	9.25	10.11 (9.43)	10.25 (9.91)	11.27 (10.79)	8.62 (8.52)	10.13	10.03	10.30	9.99	9.92
	Val.	10.02	9.82	10.39 (9.83)	10.72 (10.40)	11.23 (10.77)	8.80 (8.72)	10.41	10.30	10.60	10.12	10.06
	Ryd.	12.12	12.08	11.04 (11.00)	11.88 (11.85)	11.86 (11.83)	11.16 (11.13)	11.48	11.32	11.11	11.22	10.95
C ₂ H ₂	Ryd.	12.72	12.71	11.72 (11.65)	12.39 (12.37)	12.45 (12.42)	11.81 (11.80)	11.71	11.83	11.63	11.75	11.52
	Ryd.	12.82	12.81	11.69 (11.62)	12.37 (12.32)	12.46 (12.41)	11.68 (11.67)	12.06	12.03	11.83	11.96	11.72
	Val.	6.27	5.90	7.95 (7.33)	7.37 (7.05)	8.09 (7.67)	5.72 (5.63)	7.28	7.24	7.26	7.15	7.10
	Val.	6.61	6.42	8.15 (7.59)	7.74 (7.46)	8.17 (7.81)	5.94 (5.87)	7.62	7.56	7.59	7.48	7.44
	Ryd.	7.15	7.13	7.41 (7.31)	7.64 (7.62)	7.69 (7.66)	7.01 (6.98)	7.35	7.34	7.29	7.42	7.39
	Val.	7.72	7.37	8.36 (8.11)	8.19 (8.04)	8.34 (8.31)	7.02 (6.97)	7.95	7.91	7.92	8.02	7.93
CH ₂ O	Ryd.	7.74	7.73	8.04 (7.97)	8.29 (8.26)	8.35 (8.35)	7.64 (7.61)	8.01	7.99	7.95	8.08	8.08
	Val.	4.57	4.39	4.82 (4.26)	5.03 (4.68)	5.66 (5.17)	2.78 (2.68)	4.04	3.92	4.07	4.01	3.98
	Ryd.	8.59	8.59	6.36 (6.40)	7.87 (7.85)	7.87 (7.88)	7.11 (7.09)	6.64	6.50	6.56	7.23	7.23
	Ryd.	9.41	9.40	7.50 (7.45)	8.76 (8.72)	8.83 (8.79)	7.87 (7.85)	7.56	7.53	7.57	8.12	8.13
	Ryd.	9.53	9.58	7.39 (7.41)	8.85 (8.84)	8.85 (8.86)	8.12 (8.11)	8.16	7.47	7.52	8.21	8.23
	Ryd.	10.02	10.02	7.40 (7.37)	8.87 (8.85)	8.92 (8.89)	8.00 (7.99)	8.04	7.99	8.04	8.65	8.67
Val.	9.82	9.57	10.00 (9.34)	10.19 (9.77)	11.00 (10.48)	7.54 (7.44)	9.38	9.17	9.32	9.28	9.22	
Val.	9.72	9.21	9.95 (9.82)	10.06 (9.82)	10.39 (10.14)	8.38 (8.31)	9.08	9.46	9.54	9.67	9.43	
MAE		0.92	0.94	0.52 (0.35)	0.64 (0.50)	0.96 (0.76)	0.69 (0.74)	0.43	0.24	0.25	0.15	
MSE		0.54	0.38	0.15 (-0.13)	0.64 (0.48)	0.96 (0.76)	-0.60 (-0.66)	0.14	0.02	0.03	0.14	
RMSE		1.06	1.09	0.63 (0.47)	0.71 (0.58)	1.06 (0.82)	0.92 (0.98)	0.55	0.33	0.33	0.20	
Max		1.92	2.02	1.27 (1.30)	1.08 (0.91)	1.94 (1.40)	1.82 (1.93)	1.77	0.76	0.71	0.44	
MAE	Val.	0.63	0.74	0.66 (0.23)	0.61 (0.32)	1.27 (0.84)	1.34 (1.44)	0.26	0.17	0.23	0.09	
MSE	Val.	-0.20	-0.52	0.66 (0.06)	0.61 (0.27)	1.27 (0.84)	-1.34 (-1.44)	0.20	0.14	0.23	0.09	
RMSE	Val.	0.75	0.94	0.70 (0.26)	0.69 (0.41)	1.35 (0.91)	1.37 (1.47)	0.30	0.22	0.30	0.11	
Max	Val.	1.45	2.02	0.99 (0.49)	1.08 (0.71)	1.94 (1.40)	1.82 (1.93)	0.56	0.50	0.57	0.24	
MAE	Ryd.	1.16	1.12	0.43 (0.45)	0.68 (0.64)	0.75 (0.71)	0.23 (0.23)	0.47	0.30	0.27	0.19	
MSE	Ryd.	1.09	1.04	-0.24 (-0.30)	0.68 (0.64)	0.75 (0.71)	-0.07 (-0.09)	0.22	-0.07	-0.13	0.19	
RMSE	Ryd.	1.26	1.22	0.59 (0.59)	0.73 (0.69)	0.80 (0.76)	0.31 (0.31)	0.54	0.41	0.36	0.25	
Max	Ryd.	1.92	1.84	1.27 (1.30)	0.95 (0.91)	1.07 (1.00)	0.67 (0.68)	1.06	0.76	0.71	0.44	

excitations. This highlights the key role of the excitonic effect (*i.e.*, the attractive interaction of the excited electron and the hole left behind), which is captured by the BSE kernel and is crucial for an accurate description of neutral excitations. Importantly, BSE@GF2 (MAE and MSE of 0.52 eV and 0.15 eV, respectively) provides better excitation energies for singlet states compared to BSE@GW (MAE and MSE of 0.64 eV), as indicated by their respective statistical descriptors. This observation suggests that the versatility of the GF2 kernel, which contains ph, hp, pp, and hh terms, is a key factor behind its superior performance in describing singlet excitations (see Sec. III B). However, these trends might be different for larger chemical systems where screening effects become predominant. Furthermore, while BSE@GF2 exhibits a similar accuracy to the second-order method CIS(D) for singlet excitations, BSE@GW outperforms BSE@GF2 for triplet excitations. Another notable observation is that the static GF2 kernel provides a better description of Rydberg excitations compared to valence states. Conversely, the static GW kernel performs bet-

ter for valence than Rydberg excitations. These hold for both singlet and triplet transitions. A last point worth highlighting is the contrasted performance of BSE@GT for the two classes of excitations: while the accuracy of BSE@GT is poor for the valence states (MAEs of 1.34 eV and 1.50 eV for singlets and triplets, respectively), it can be considered accurate for Rydberg transitions (MAEs of 0.23 eV and 0.31 eV for singlets and triplets, respectively), where the excited-state density is much lower than the ground-state one, a situation where ladder diagrams are known to be relevant (see Sec. II D).

By taking into account the dynamical corrections, we observe an overall improvement in the description of both singlet and triplet excitations, except at the BSE@GT level. From a general point of view, as previously mentioned and analyzed in Refs. 161, Rydberg excitations are less affected by dynamical effects than valence excitations across all BSE kernels. For singlet excitations, dBSE@GF2 outperforms CIS(D), especially for singlet valence excitations where its performance surpasses that of all second-order methods, except for EOM-CCSD,

TABLE III. Triplet excitation energies (in eV) of various molecules computed using the aug-cc-pVTZ basis set at different levels of theory. The dynamically-corrected BSE transition energies (dBSE) are reported in parentheses. The statistical descriptors associated with the errors with respect to the reference values are also reported for the entire dataset and separately for valence (Val.) and Rydberg (Ryd.) excited states.

Mol.	Nature	CIS	TDHF	BSE@GF2	BSE@GW	BSE@GT	CIS(D)	ADC(2)	CC2	CCSD	TBE			
H ₂ O	Ryd.	8.00	7.88	7.02	(6.80)	7.62	(7.48)	6.60	(6.54)	7.25	6.86	6.91	7.20	6.92
	Ryd.	10.01	9.88	8.68	(8.60)	9.61	(9.50)	8.65	(8.58)	9.24	8.72	8.77	9.20	8.91
N ₂	Ryd.	10.10	9.87	9.33	(9.09)	9.81	(9.67)	8.82	(8.75)	9.54	9.15	9.20	9.49	9.30
	Val.	6.16	3.36	8.88	(7.41)	8.03	(7.38)	6.17	(5.91)	8.20	8.15	8.19	7.66	7.70
	Val.	7.95	7.57	9.04	(8.10)	8.66	(8.10)	6.30	(6.12)	8.33	8.20	8.19	8.09	8.01
	Val.	7.23	5.72	9.94	(8.67)	9.04	(8.48)	7.11	(6.90)	9.30	9.25	9.30	8.91	8.87
CO	Val.	8.43	7.86	10.91	(9.88)	10.11	(9.66)	7.99	(7.85)	10.29	10.23	10.29	9.83	9.66
	Val.	5.81	5.22	7.59	(6.45)	6.80	(6.25)	4.99	(4.76)	6.51	6.45	6.42	6.36	6.28
	Val.	7.68	6.21	8.80	(7.71)	8.57	(8.07)	7.02	(6.81)	8.63	8.54	8.72	8.34	8.45
	Val.	8.61	7.71	9.58	(8.68)	9.39	(8.96)	7.78	(7.62)	9.44	9.33	9.56	9.23	9.27
	Val.	9.61	9.25	10.24	(9.56)	10.25	(9.91)	8.49	(8.39)	10.10	10.01	10.27	9.81	9.80
	Ryd.	11.13	11.03	10.86	(10.71)	11.17	(11.07)	10.48	(10.41)	10.98	10.83	10.60	10.71	10.47
C ₂ H ₂	Val.	4.51	2.16	7.09	(6.13)	5.83	(5.32)	4.18	(3.99)	5.79	5.75	5.76	5.45	5.53
	Val.	5.41	4.44	7.60	(6.81)	6.64	(6.24)	4.97	(4.83)	6.62	6.57	6.60	6.41	6.40
	Val.	6.27	5.90	8.05	(7.43)	7.37	(7.05)	5.66	(5.57)	7.31	7.27	7.29	7.12	7.08
C ₂ H ₄	Val.	3.61	0.76	6.15	(5.20)	4.96	(4.50)	3.15	(2.07)	4.62	4.59	4.59	4.46	4.54
	Ryd.	6.92	6.88	7.40	(7.25)	7.46	(7.42)	6.83	(6.07)	7.26	7.23	7.19	7.29	7.23
CH ₂ O	Ryd.	7.65	7.62	8.04	(7.96)	8.23	(8.19)	7.58	(7.17)	7.97	7.95	7.91	8.03	7.98
	Val.	3.75	3.40	4.52	(3.83)	4.28	(3.88)	2.17	(2.02)	3.58	3.46	3.59	3.56	3.58
	Val.	4.88	1.95	5.96	(4.31)	6.32	(5.76)	4.26	(4.03)	6.27	6.20	6.30	5.97	6.06
Max	Ryd.	8.25	8.17	6.32	(6.28)	7.60	(7.56)	6.79	(6.75)	6.66	6.39	6.44	7.08	7.06
MAE		0.82	1.65	0.72	(0.39)	0.41	(0.27)	1.10	(1.33)	0.27	0.21	0.24	0.10	
MSE		-0.34	-1.25	0.61	(-0.11)	0.41	(0.06)	-1.10	(-1.33)	0.23	0.10	0.14	0.05	
RMSE		0.92	2.10	0.88	(0.54)	0.46	(0.33)	1.25	(1.48)	0.31	0.27	0.30	0.13	
Max		1.64	4.34	1.61	(1.75)	0.70	(0.60)	1.80	(2.47)	0.63	0.67	0.63	0.29	
MAE	Val.	0.83	2.12	0.95	(0.47)	0.36	(0.19)	1.50	(1.74)	0.27	0.21	0.27	0.06	
MSE	Val.	-0.81	-2.12	0.94	(-0.08)	0.36	(-0.12)	-1.50	(-1.74)	0.27	0.20	0.27	-0.00	
RMSE	Val.	0.96	2.52	1.06	(0.62)	0.40	(0.23)	1.51	(1.76)	0.31	0.26	0.32	0.08	
Max	Val.	1.64	4.34	1.61	(1.75)	0.70	(0.39)	1.80	(2.47)	0.63	0.57	0.63	0.17	
MAE	Ryd.	0.78	0.70	0.25	(0.24)	0.52	(0.43)	0.31	(0.51)	0.26	0.21	0.16	0.16	
MSE	Ryd.	0.60	0.49	-0.03	(-0.17)	0.52	(0.43)	-0.30	(-0.51)	0.15	-0.11	-0.12	0.16	
RMSE	Ryd.	0.85	0.75	0.34	(0.34)	0.55	(0.46)	0.34	(0.62)	0.32	0.30	0.25	0.19	
Max	Ryd.	1.19	1.11	0.74	(0.78)	0.70	(0.60)	0.48	(1.16)	0.51	0.67	0.62	0.29	

which is known to be highly accurate for small molecular systems.^{246,247} Although dBSE@GW shows an improvement compared to its static version, it does not reach the accuracy of dBSE@GF2 or second-order methods. However, for triplet excitations, dBSE@GW is on par with CIS(D), ADC(2), CC2, and EOM-CCSD, while dBSE@GF2 falls short of the accuracy of CIS(D). In particular, for triplet valence excitations, dBSE@GW outperforms all second-order methods, except EOM-CCSD. For these small molecular systems, both at the static and dynamic levels, the second-order scheme BSE2@GW does not bring any improvement upon its first-order version.

C. Singlet-triplet gap of cycl[3,3,3]zinc

Molecules with an inverted singlet-triplet gap (*i.e.*, where the lowest singlet excited state is higher in energy than the lowest triplet state) are of particular interest in TADF^{248,249} because they can harness both singlet and triplet excitons for emission, thereby enhancing the efficiency of OLEDs.^{250,251} Thanks to this inverted gap, the system can undergo efficient reverse intersystem crossing, a process in which the population from the triplet state can be thermally activated and transferred back to the singlet state, resulting in delayed fluorescence.

TABLE IV. Lowest singlet and triplet vertical excitation energies, E_S and E_T , and resulting singlet-triplet gap ΔE_{ST} (in eV) of cycl[3,3,3]zinc computed at various levels of theory using the cc-pVDZ basis. The percentage of single excitations involved in each transition, % T_1 , computed at the EOM-CC3 level is reported in parenthesis.

Method	E_S	E_T	ΔE_{ST}
CIS	1.83	1.50	+0.33
TDHF	1.68	1.08	+0.60
BSE@GW	1.25	0.97	+0.28
dBSE@GW	1.16	0.84	+0.32
BSE2@GW	0.99	0.97	+0.02
dBSE2@GW	0.67	0.84	-0.17
CIS(D)	1.07	1.37	-0.30
ADC(2)	1.04	1.20	-0.16
ADC(3)	0.78	0.87	-0.09
EOM-CC2	1.09	1.25	-0.16
EOM-CCSD	1.09	1.19	-0.10
EOM-CC3	0.98(87%)	1.15(96%)	-0.17

Recently, such systems have been scrutinized at different computational levels, including TD-DFT and second-order wave function methods, such as CIS(D), ADC(2), and EOM-CCSD.²⁵²⁻²⁵⁸ In particular, de Silva has shown that this inversion requires a substantial contribution from the double excitations.²⁵² This explains why adi-

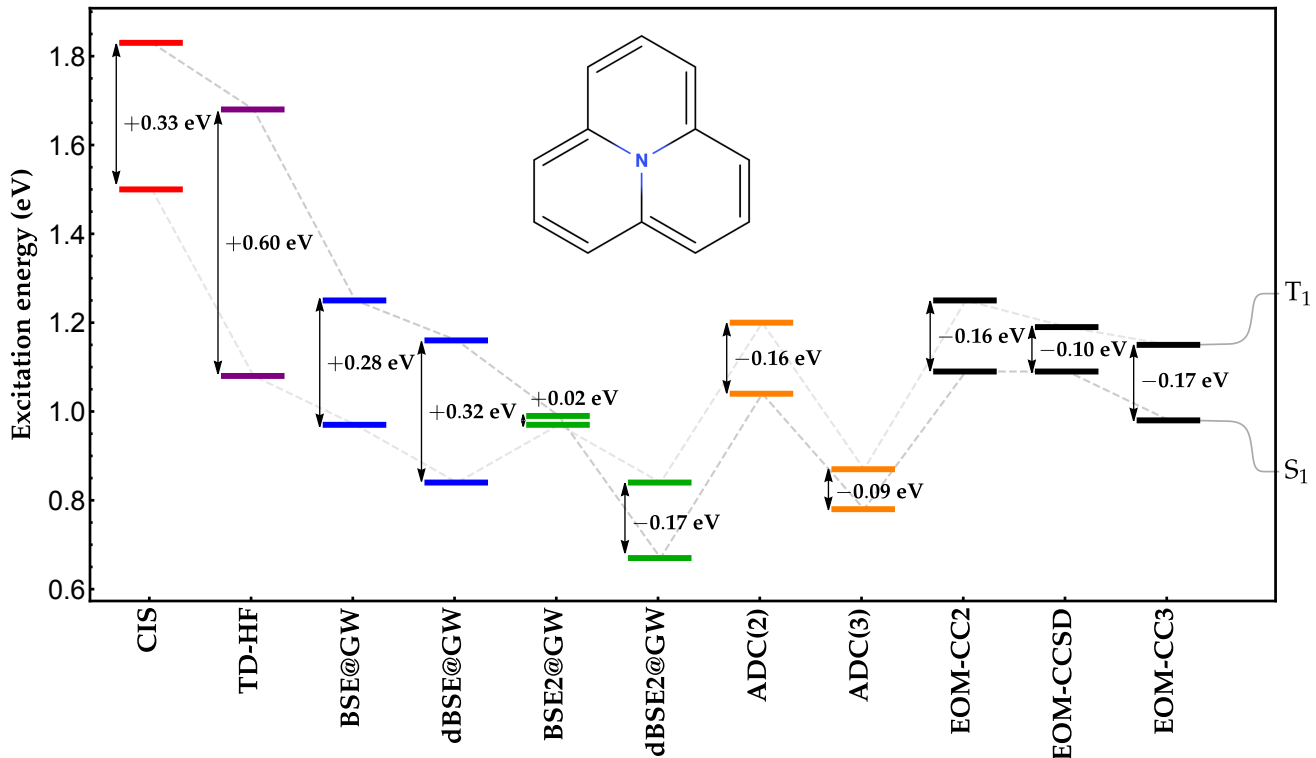


FIG. 1. Evolution of the lowest singlet and triplet vertical excitation energies (in eV) of cycl[3,3,3]zine evaluated with different computational methods using the cc-pVDZ basis.

abatic TD-DFT is not able to reproduce this particular feature, and second- or higher-order methods are required where double excitations are explicitly treated.

Following the computational protocol of Ref. 252, we compute the lowest singlet and triplet excitation energies, E_S and E_T , as well as the corresponding singlet-triplet gap, ΔE_{ST} , of cycl[3,3,3]zine (see Fig. 1), a model molecular emitter for TADF, with the cc-pVDZ basis at various levels of theory. The geometry of cycl[3,3,3]zine has been optimized at the B3LYP/cc-pVDZ level and is reported in [supplementary material](#) for the sake of completeness. Additionally, we have been able to compute the singlet-triplet gap with third-order methods such as ADC(3)^{201,259,260} and EOM-CC3.^{261,262}

Our results are gathered in Table IV and shown in Fig. 1. As expected, the BSE@GW and BSE2@GW calculations do not produce an inverted singlet-triplet gap due to the static nature of the kernel. Because the dynamical correction of the singlet and triplet excitation energies cancel each other pretty much exactly, dBSE@GW yields the same state ordering. However, the second-order dynamical GW kernel (which only corrects singlet states as explained in Sec. III D) faithfully predicts this inversion although the corresponding excitation energies are underestimated compared to other approaches, except ADC(3), which is known to exhibit this trend.²⁶³ Interestingly, ADC(2), EOM-CC2, EOM-CC3, and BSE2@GW yield essentially the same value, while EOM-CCSD and ADC(3) slightly underestimate

the gap. Because the percentage of single excitations involved in these two valence transitions ($\%T_1$, see Table IV) is high (although not negligible for the singlet state), the EOM-CC3 value is likely to be accurate.²⁴⁷ Note that, because of the poor quality of the GF2 quasiparticle energies, we could not compute excitation energies at the (d)BSE@GF2 level as spurious poles appeared in the BSE kernel.

VI. CONCLUDING REMARKS

In this study, our focus was on examining the relationships between different Green’s function methods, specifically exploring various approximations for the self-energy (GF2, GW, and GT) and their corresponding BSE kernels at the static and dynamic levels. Additionally, we extended the unfolding process, previously confined to the GF2 and GW frameworks, to the T -matrix approximation. The introduction of this unfolding framework allowed us to uncover connections between GF2 and the ADC(2) scheme concerning both charged and neutral excitations, and to propose new directions for the development of accurate kernels at the GW level.

Subsequently, we applied these three distinct approximations to calculate the principal IPs and vertical transition energies for both singlet and triplet states of small molecules. Our findings can be summarized as follows:

- Confirming previous knowledge, the *GW* approximation surpasses the GF2 method in accurately calculating IPs, emphasizing the significance of screening even in small molecular systems.
- The *T*-matrix approximation exhibits comparable accuracy to *GW*, although it falls slightly short.
- For the singlet excited states of small molecules, the GF2 kernel generally outperforms its *GW* counterpart. Conversely, for triplet excitations, BSE@*GW* provides more accurate vertical excitation energies.
- Importantly, our investigations highlight the sensitivity of BSE kernels to the nature of the excited states. For example, BSE@*GT* is poor for valence states while it is accurate for Rydberg transitions.
- Overall, except in the *T*-matrix approximation, dynamical corrections are almost systematically beneficial.

It is important to note that these conclusions are drawn specifically for small molecules, and it would be intriguing to explore if similar trends persist in larger systems.

To initiate our pursuit of this objective, we examined the capability of our various schemes to replicate the inversion of the singlet-triplet gap in cycl[3,3,3]zine, a prototypical molecular emitter for TADF. With the exception of one case, we observed that all static and dynamic BSE-based schemes failed to reproduce this unique characteristic. The only exception was the dynamically-corrected BSE2@*GW* scheme, which yielded a gap value consistent with that obtained from EOM-CC3 calculations. This observation effectively highlights the significance of higher-order terms and dynamic effects within the BSE formalism, and we anticipate that these findings will stimulate further advancements in this area of research.

SUPPLEMENTARY MATERIAL

See the supplementary material for linearized *vs* dynamical quasiparticle energies of the *GW*20 set in the cc-pVDZ basis, TDHF@GF2, TDHF@*GW*, and TDHF@*GT* singlet excitation energies in the aug-cc-pVTZ basis, and optimize ground-state geometry of the cycl[3,3,3]zine molecule at the B3LYP/cc-pVDZ level.

ACKNOWLEDGMENTS

The authors thank Pina Romaniello, Fabien Bruneval, and Xavier Blase for insightful discussions. They also thank Antoine Marie for useful comments on this manuscript. This work used the HPC resources from CALMIP (Toulouse) under allocation 2023-18005. This project has received funding from the European Research Council (ERC) under the European Union’s Horizon

2020 research and innovation programme (Grant agreement No. 863481).

DATA AVAILABILITY STATEMENT

The data that supports the findings of this study are available within the article and its supplementary material.

- ¹G. Csanak, H. Taylor, and R. Yaris, in *Advances in atomic and molecular physics*, Vol. 7 (Elsevier, 1971) pp. 287–361.
- ²A. L. Fetter and J. D. Waleck, *Quantum Theory of Many Particle Systems* (McGraw Hill, San Francisco, 1971).
- ³R. M. Martin, L. Reining, and D. M. Ceperley, *Interacting Electrons: Theory and Computational Approaches* (Cambridge University Press, 2016).
- ⁴F. Bruneval, T. Rangel, S. M. Hamed, M. Shao, C. Yang, and J. B. Neaton, *Comput. Phys. Commun.* **208**, 149 (2016).
- ⁵D. Golze, M. Dvorak, and P. Rinke, *Front. Chem.* **7**, 377 (2019).
- ⁶X. Blase, I. Duchemin, and D. Jacquemin, *Chem. Soc. Rev.* **47**, 1022 (2018).
- ⁷X. Blase, I. Duchemin, D. Jacquemin, and P.-F. Loos, *J. Phys. Chem. Lett.* **11**, 7371 (2020).
- ⁸J. Schirmer, *Many-Body Methods for Atoms, Molecules and Clusters* (Springer, 2018).
- ⁹G. Das, *J. Chem. Phys.* **58**, 5104 (1973).
- ¹⁰E. Dalgaard and P. Jørgensen, *J. Chem. Phys.* **69**, 3833 (1978).
- ¹¹B. H. Lengsfeld, *J. Chem. Phys.* **73**, 382 (1980).
- ¹²C. W. Bauschlicher and D. R. Yarkony, *J. Chem. Phys.* **72**, 1138 (1980).
- ¹³C. W. Bauschlicher, D. M. Silver, and D. R. Yarkony, *J. Chem. Phys.* **73**, 2867 (1980).
- ¹⁴H. Werner and W. Meyer, *J. Chem. Phys.* **74**, 5794 (1981).
- ¹⁵J. T. Golab, D. L. Yeager, and P. Jørgensen, *Chem. Phys.* **78**, 175 (1983).
- ¹⁶T. Ziegler, A. Rauk, and E. Baerends, *Theor. Chim. Acta* **43**, 261 (1977).
- ¹⁷T. Kowalczyk, S. Yost, and T. Voorhis, *Chem. Phys.* **134**, 054128 (2011).
- ¹⁸F. Aryasetiawan and O. Gunnarsson, *Rep. Prog. Phys.* **61**, 237 (1998).
- ¹⁹G. Onida, L. Reining, and A. Rubio, *Rev. Mod. Phys.* **74**, 601 (2002).
- ²⁰L. Reining, *Wiley Interdiscip. Rev. Comput. Mol. Sci.* **8**, e1344 (2017).
- ²¹F. Bruneval, N. Dattani, and M. J. van Setten, *Front. Chem.* **9**, 749779 (2021).
- ²²G. Strinati, H. J. Mattausch, and W. Hanke, *Phys. Rev. Lett.* **45**, 290 (1980).
- ²³G. Strinati, H. J. Mattausch, and W. Hanke, *Phys. Rev. B* **25**, 2867 (1982).
- ²⁴G. Strinati, *Phys. Rev. Lett.* **49**, 1519 (1982).
- ²⁵M. S. Hybertsen and S. G. Louie, *Phys. Rev. Lett.* **55**, 1418 (1985).
- ²⁶M. S. Hybertsen and S. G. Louie, *Phys. Rev. B* **34**, 5390 (1986).
- ²⁷R. W. Godby, M. Schlüter, and L. J. Sham, *Phys. Rev. Lett.* **56**, 2415 (1986).
- ²⁸R. W. Godby, M. Schlüter, and L. J. Sham, *Phys. Rev. B* **36**, 6497 (1987).
- ²⁹R. W. Godby, M. Schlüter, and L. J. Sham, *Phys. Rev. B* **35**, 4170 (1987).
- ³⁰R. W. Godby, M. Schlüter, and L. J. Sham, *Phys. Rev. B* **37**, 10159 (1988).
- ³¹X. Blase, A. Rubio, S. G. Louie, and M. L. Cohen, *Phys. Rev. B* **51**, 6868 (1995).
- ³²M. Rohlfing and S. G. Louie, *Phys. Rev. Lett.* **82**, 1959 (1999).
- ³³J.-W. van der Horst, P. A. Bobbert, M. A. J. Michels, G. Brocks, and P. J. Kelly, *Phys. Rev. Lett.* **83**, 4413 (1999).

- ³⁴P. Puschnig and C. Ambrosch-Draxl, *Phys. Rev. Lett.* **89**, 056405 (2002).
- ³⁵M. L. Tiago, J. E. Northrup, and S. G. Louie, *Phys. Rev. B* **67**, 115212 (2003).
- ³⁶D. Rocca, D. Lu, and G. Galli, *J. Chem. Phys.* **133**, 164109 (2010).
- ³⁷P. Boulanger, D. Jacquemin, I. Duchemin, and X. Blase, *J. Chem. Theory Comput.* **10**, 1212 (2014).
- ³⁸D. Jacquemin, I. Duchemin, and X. Blase, *J. Chem. Theory Comput.* **11**, 3290 (2015).
- ³⁹F. Bruneval, S. M. Hamed, and J. B. Neaton, *J. Chem. Phys.* **142**, 244101 (2015).
- ⁴⁰D. Jacquemin, I. Duchemin, and X. Blase, *J. Chem. Theory Comput.* **11**, 5340 (2015).
- ⁴¹D. Hirose, Y. Noguchi, and O. Sugino, *Phys. Rev. B* **91**, 205111 (2015).
- ⁴²D. Jacquemin, I. Duchemin, and X. Blase, *J. Phys. Chem. Lett.* **8**, 1524 (2017).
- ⁴³D. Jacquemin, I. Duchemin, A. Blondel, and X. Blase, *J. Chem. Theory Comput.* **13**, 767 (2017).
- ⁴⁴T. Rangel, S. M. Hamed, F. Bruneval, and J. B. Neaton, *J. Chem. Phys.* **146**, 194108 (2017).
- ⁴⁵K. Krause and W. Klopper, *J. Comput. Chem.* **38**, 383 (2017).
- ⁴⁶X. Gui, C. Holzer, and W. Klopper, *J. Chem. Theory Comput.* **14**, 2127 (2018).
- ⁴⁷C. Liu, J. Kloppenburg, Y. Yao, X. Ren, H. Appel, Y. Kanai, and V. Blum, *J. Chem. Phys.* **152**, 044105 (2020).
- ⁴⁸J. Li, M. Holzmann, I. Duchemin, X. Blase, and V. Olevano, *Phys. Rev. Lett.* **118**, 163001 (2017).
- ⁴⁹J. Li, N. D. Drummond, P. Schuck, and V. Olevano, *SciPost Phys.* **6**, 040 (2019).
- ⁵⁰J. Li, I. Duchemin, X. Blase, and V. Olevano, *SciPost Phys.* **8**, 20 (2020).
- ⁵¹J. Li and V. Olevano, *Phys. Rev. A* **103**, 012809 (2021).
- ⁵²C. Holzer and W. Klopper, *J. Chem. Phys.* **149**, 101101 (2018).
- ⁵³C. Holzer, X. Gui, M. E. Harding, G. Kresse, T. Helgaker, and W. Klopper, *J. Chem. Phys.* **149**, 144106 (2018).
- ⁵⁴P.-F. Loos, A. Scemama, I. Duchemin, D. Jacquemin, and X. Blase, *J. Phys. Chem. Lett.* **11**, 3536 (2020).
- ⁵⁵P.-F. Loos, M. Comin, X. Blase, and D. Jacquemin, *J. Chem. Theory Comput.* **17**, 3666 (2021).
- ⁵⁶C. A. McKeon, S. M. Hamed, F. Bruneval, and J. B. Neaton, *J. Chem. Phys.* **157**, 074103 (2022).
- ⁵⁷M. J. van Setten, R. Costa, F. Viñes, and F. Illas, *J. Chem. Theory Comput.* **14**, 877 (2018).
- ⁵⁸Y. Jin, N. Q. Su, and W. Yang, *J. Phys. Chem. Lett.* **10**, 447 (2019).
- ⁵⁹Y. Jin and W. Yang, *J. Phys. Chem. A* **123**, 3199 (2019).
- ⁶⁰D. Golze, J. Wilhelm, M. J. van Setten, and P. Rinke, *J. Chem. Theory Comput.* **14**, 4856 (2018).
- ⁶¹D. Golze, L. Keller, and P. Rinke, *J. Phys. Chem. Lett.* **11**, 1840 (2020).
- ⁶²J. Li, Y. Jin, P. Rinke, W. Yang, and D. Golze, *J. Chem. Theory Comput.* **18**, 7570 (2022).
- ⁶³J. Li, D. Golze, and W. Yang, *J. Chem. Theory Comput.* **18**, 6637 (2022).
- ⁶⁴J. Li and W. Yang, *J. Phys. Chem. Lett.* **13**, 9372 (2022).
- ⁶⁵A. Förster and L. Visscher, *J. Chem. Theory Comput.* **18**, 6779 (2022).
- ⁶⁶M. E. Casida and D. P. Chong, *Phys. Rev. A* **40**, 4837 (1989).
- ⁶⁷M. E. Casida and D. P. Chong, *Phys. Rev. A* **44**, 5773 (1991).
- ⁶⁸J. V. Ortiz, *Wiley Interdiscip. Rev. Comput. Mol. Sci.* **3**, 123 (2013).
- ⁶⁹J. J. Phillips and D. Zgid, *J. Chem. Phys.* **140**, 241101 (2014).
- ⁷⁰J. J. Phillips, A. A. Kananenka, and D. Zgid, *J. Chem. Phys.* **142**, 194108 (2015).
- ⁷¹A. A. Rusakov, J. J. Phillips, and D. Zgid, *J. Chem. Phys.* **141**, 194105 (2014).
- ⁷²A. A. Rusakov and D. Zgid, *J. Chem. Phys.* **144**, 054106 (2016).
- ⁷³S. Hirata, M. R. Hermes, J. Simons, and J. V. Ortiz, *J. Chem. Theory Comput.* **11**, 1595 (2015).
- ⁷⁴S. Hirata, A. E. Doran, P. J. Knowles, and J. V. Ortiz, *J. Chem. Phys.* **147**, 044108 (2017).
- ⁷⁵O. J. Backhouse, A. Santana-Bonilla, and G. H. Booth, *J. Phys. Chem. Lett.* **12**, 7650 (2021).
- ⁷⁶O. J. Backhouse and G. H. Booth, *J. Chem. Theory Comput.* **16**, 6294 (2020).
- ⁷⁷O. J. Backhouse, M. Nusspickel, and G. H. Booth, *J. Chem. Theory Comput.* **16**, 1090 (2020).
- ⁷⁸P. Pokhilko and D. Zgid, *J. Chem. Phys.* **155**, 024101 (2021).
- ⁷⁹P. Pokhilko, S. Iskakov, C.-N. Yeh, and D. Zgid, *J. Chem. Phys.* **155**, 024119 (2021).
- ⁸⁰P. Pokhilko, C.-N. Yeh, and D. Zgid, *J. Chem. Phys.* **156**, 094101 (2022).
- ⁸¹G. Stefanucci and R. van Leeuwen, *Nonequilibrium Many-Body Theory of Quantum Systems: A Modern Introduction* (Cambridge University Press, Cambridge, 2013).
- ⁸²A. Liebsch, *Phys. Rev. B* **23**, 5203 (1981).
- ⁸³N. E. Bickers, D. J. Scalapino, and S. R. White, *Phys. Rev. Lett.* **62**, 961 (1989).
- ⁸⁴N. E. Bickers and S. R. White, *Phys. Rev. B* **43**, 8044 (1991).
- ⁸⁵M. I. Katsnelson and A. I. Lichtenstein, *J. Phys. Condens. Matter* **11**, 1037 (1999).
- ⁸⁶M. Katsnelson and A. Lichtenstein, *Eur. Phys. J. B* **30**, 9 (2002).
- ⁸⁷V. P. Zhukov, E. V. Chulkov, and P. M. Echenique, *Phys. Rev. B* **72**, 72.155109 (2005).
- ⁸⁸M. Puig von Friesen, C. Verdozzi, and C.-O. Almbladh, *Phys. Rev. B* **82**, 155108 (2010).
- ⁸⁹P. Romaniello, F. Bechstedt, and L. Reining, *Phys. Rev. B* **85**, 155131 (2012).
- ⁹⁰J. Gukelberger, L. Huang, and P. Werner, *Phys. Rev. B* **91**, 235114 (2015).
- ⁹¹M. C. T. D. Müller, S. Blügel, and C. Friedrich, *Phys. Rev. B* **100**, 045130 (2019).
- ⁹²C. Friedrich, *Phys. Rev. B* **100**, 075142 (2019).
- ⁹³T. Biswas and A. Singh, *npj Comput. Mater.* **7**, 189 (2021).
- ⁹⁴D. Zhang, N. Q. Su, and W. Yang, *J. Phys. Chem. Lett.* **8**, 3223 (2017).
- ⁹⁵J. Li, Z. Chen, and W. Yang, *J. Phys. Chem. Lett.* **12**, 6203 (2021).
- ⁹⁶P.-F. Loos and P. Romaniello, *J. Chem. Phys.* **156**, 164101 (2022).
- ⁹⁷H. A. Bethe and J. Goldstone, *Proc. Math. Phys. Eng. Sci.* **238**, 551 (1957).
- ⁹⁸G. Baym and L. P. Kadanoff, *Phys. Rev.* **124**, 287 (1961).
- ⁹⁹G. Baym, *Phys. Rev.* **127**, 1391 (1962).
- ¹⁰⁰P. Danielewicz, *Ann. Phys.* **152**, 239 (1984).
- ¹⁰¹P. Danielewicz, *Ann. Phys.* **152**, 305 (1984).
- ¹⁰²C. De Dominicis and P. C. Martin, *J. Math. Phys.* **5**, 14 (1964).
- ¹⁰³C. De Dominicis and P. C. Martin, *J. Math. Phys.* **5**, 31 (1964).
- ¹⁰⁴N. Bickers and D. Scalapino, *Ann. Phys.* **193**, 206 (1989).
- ¹⁰⁵L. Hedin, *J. Phys. Condens. Matter* **11**, R489 (1999).
- ¹⁰⁶N. E. Bickers, “Self-consistent many-body theory for condensed matter systems,” in *Theoretical Methods for Strongly Correlated Electrons*, edited by D. Sénéchal, A.-M. Tremblay, and C. Bourbonnais (Springer New York, 2004) pp. 237–296.
- ¹⁰⁷E. L. Shirley, *Phys. Rev. B* **54**, 7758 (1996).
- ¹⁰⁸R. Del Sole, L. Reining, and R. W. Godby, *Phys. Rev. B* **49**, 8024 (1994).
- ¹⁰⁹A. Schindlmayr and R. W. Godby, *Phys. Rev. Lett.* **80**, 1702 (1998).
- ¹¹⁰A. J. Morris, M. Stankovski, K. T. Delaney, P. Rinke, P. García-González, and R. W. Godby, *Phys. Rev. B* **76**, 155106 (2007).
- ¹¹¹M. Shishkin, M. Marsman, and G. Kresse, *Phys. Rev. Lett.* **99**, 246403 (2007).
- ¹¹²P. Romaniello, S. Guyot, and L. Reining, *J. Chem. Phys.* **131**, 154111 (2009).
- ¹¹³A. Grüneis, G. Kresse, Y. Hinuma, and F. Oba, *Phys. Rev. Lett.* **112**, 096401 (2014).

- ¹¹⁴L. Hung, F. Bruneval, K. Baishya, and S. Ögüt, *J. Chem. Theory Comput.* **13**, 2135 (2017).
- ¹¹⁵E. Maggio and G. Kresse, *J. Chem. Theory Comput.* **13**, 4765 (2017).
- ¹¹⁶C. Mejuto-Zaera and V. c. v. Vlček, *Phys. Rev. B* **106**, 165129 (2022).
- ¹¹⁷M. S. Hybertsen and S. G. Louie, *Phys. Rev. Lett.* **55**, 1418 (1985).
- ¹¹⁸W. von der Linden and P. Horsch, *Phys. Rev. B* **37**, 8351 (1988).
- ¹¹⁹J. E. Northrup, M. S. Hybertsen, and S. G. Louie, *Phys. Rev. Lett.* **66**, 500 (1991).
- ¹²⁰X. Blase, X. Zhu, and S. G. Louie, *Phys. Rev. B* **49**, 4973 (1994).
- ¹²¹M. Rohlfing, P. Krüger, and J. Pollmann, *Phys. Rev. B* **52**, 1905 (1995).
- ¹²²M. Shishkin and G. Kresse, *Phys. Rev. B* **75**, 235102 (2007).
- ¹²³X. Blase and C. Attaccalite, *Appl. Phys. Lett.* **99**, 171909 (2011).
- ¹²⁴C. Faber, C. Attaccalite, V. Olevano, E. Runge, and X. Blase, *Phys. Rev. B* **83**, 115123 (2011).
- ¹²⁵T. Rangel, S. M. Hamed, F. Bruneval, and J. B. Neaton, *J. Chem. Theory Comput.* **12**, 2834 (2016).
- ¹²⁶S. V. Faleev, M. van Schilfhaarde, and T. Kotani, *Phys. Rev. Lett.* **93**, 126406 (2004).
- ¹²⁷M. van Schilfhaarde, T. Kotani, and S. Faleev, *Phys. Rev. Lett.* **96**, 226402 (2006).
- ¹²⁸T. Kotani, M. van Schilfhaarde, and S. V. Faleev, *Phys. Rev. B* **76**, 165106 (2007).
- ¹²⁹S.-H. Ke, *Phys. Rev. B* **84**, 205415 (2011).
- ¹³⁰F. Kaplan, M. E. Harding, C. Seiler, F. Weigend, F. Evers, and M. J. van Setten, *J. Chem. Theory Comput.* **12**, 2528 (2016).
- ¹³¹E. E. Salpeter and H. A. Bethe, *Phys. Rev.* **84**, 1232 (1951).
- ¹³²G. Strinati, *Riv. Nuovo Cimento* **11**, 1 (1988).
- ¹³³E. Runge and E. K. U. Gross, *Phys. Rev. Lett.* **52**, 997 (1984).
- ¹³⁴M. E. Casida, “Time-dependent density functional response theory for molecules,” (World Scientific, Singapore, 1995) pp. 155–192.
- ¹³⁵M. Petersilka, U. J. Gossmann, and E. K. U. Gross, *Phys. Rev. Lett.* **76**, 1212 (1996).
- ¹³⁶C. Ullrich, *Time-Dependent Density-Functional Theory: Concepts and Applications*, Oxford Graduate Texts (Oxford University Press, New York, 2012).
- ¹³⁷D. Zhang, S. N. Steinmann, and W. Yang, *J. Chem. Phys.* **139**, 154109 (2013).
- ¹³⁸E. Rebolini and J. Toulouse, *J. Chem. Phys.* **144**, 094107 (2016).
- ¹³⁹W. Dou, J. Lee, J. Zhu, L. Mejía, D. R. Reichman, R. Baer, and E. Rabani, *J. Chem. Theory Comput.* **18**, 5221 (2022).
- ¹⁴⁰P. F. Loos, P. Romaniello, and J. A. Berger, *J. Chem. Theory Comput.* **14**, 3071 (2018).
- ¹⁴¹M. Vénil, P. Romaniello, J. A. Berger, and P. F. Loos, *J. Chem. Theory Comput.* **14**, 5220 (2018).
- ¹⁴²J. A. Berger, P.-F. Loos, and P. Romaniello, *J. Chem. Theory Comput.* **17**, 191 (2020).
- ¹⁴³S. Di Sabatino, P.-F. Loos, and P. Romaniello, *Front. Chem.* **9**, 751054 (2021).
- ¹⁴⁴L. Hedin, *Phys. Rev.* **139**, A796 (1965).
- ¹⁴⁵F. Bruneval, N. Vast, and L. Reining, *Phys. Rev. B* **74**, 045102 (2006).
- ¹⁴⁶P. Koval, D. Foerster, and D. Sánchez-Portal, *Phys. Rev. B* **89**, 155417 (2014).
- ¹⁴⁷J. Wilhelm, D. Golze, L. Talirz, J. Hutter, and C. A. Pignedoli, *J. Phys. Chem. Lett.* **9**, 306 (2018).
- ¹⁴⁸A. Stan, N. E. Dahlen, and R. van Leeuwen, *Europhys. Lett.* **EPL** **76**, 298 (2006).
- ¹⁴⁹A. Stan, N. E. Dahlen, and R. van Leeuwen, *J. Chem. Phys.* **130**, 114105 (2009).
- ¹⁵⁰C. Rostgaard, K. W. Jacobsen, and K. S. Thygesen, *Phys. Rev. B* **81**, 085103 (2010).
- ¹⁵¹F. Caruso, P. Rinke, X. Ren, M. Scheffler, and A. Rubio, *Phys. Rev. B* **86**, 081102(R) (2012).
- ¹⁵²F. Caruso, P. Rinke, X. Ren, A. Rubio, and M. Scheffler, *Phys. Rev. B* **88**, 075105 (2013).
- ¹⁵³F. Caruso, *Self-Consistent GW Approach for the Unified Description of Ground and Excited States of Finite Systems*, PhD Thesis, Freie Universität Berlin (2013).
- ¹⁵⁴F. Caruso, D. R. Rohr, M. Hellgren, X. Ren, P. Rinke, A. Rubio, and M. Scheffler, *Phys. Rev. Lett.* **110**, 146403 (2013).
- ¹⁵⁵C. J. C. Scott, O. J. Backhouse, and G. H. Booth, *J. Chem. Phys.* **158**, 124102 (2023).
- ¹⁵⁶E. Monino and P.-F. Loos, *J. Chem. Phys.* **156**, 231101 (2022).
- ¹⁵⁷A. Marie and P.-F. Loos, “A similarity renormalization group approach to green’s function methods,” (2023), [arXiv:2303.05984 \[physics.chem-ph\]](https://arxiv.org/abs/2303.05984).
- ¹⁵⁸A. L. Ankudinov, A. I. Nesvizhskii, and J. J. Rehr, *Phys. Rev. B* **67**, 115120 (2003).
- ¹⁵⁹P. Romaniello, D. Sangalli, J. A. Berger, F. Sottile, L. G. Molinari, L. Reining, and G. Onida, *J. Chem. Phys.* **130**, 044108 (2009).
- ¹⁶⁰D. Sangalli, P. Romaniello, G. Onida, and A. Marini, *J. Chem. Phys.* **134**, 034115 (2011).
- ¹⁶¹P.-F. Loos and X. Blase, *J. Chem. Phys.* **153**, 114120 (2020).
- ¹⁶²J. Authier and P.-F. Loos, *J. Chem. Phys.* **153**, 184105 (2020).
- ¹⁶³B. G. Levine, C. Ko, J. Quenneville, and T. J. Martinez, *Mol. Phys.* **104**, 1039 (2006).
- ¹⁶⁴D. J. Tozer and N. C. Handy, *Phys. Chem. Chem. Phys.* **2**, 2117 (2000).
- ¹⁶⁵P. Elliott, S. Goldson, C. Canahui, and N. T. Maitra, *Chem. Phys.* **391**, 110 (2011).
- ¹⁶⁶N. T. Maitra, “Memory: History, initial-state dependence, and double-excitations,” in *Fundamentals of Time-Dependent Density Functional Theory*, Vol. 837, edited by M. A. Marques, N. T. Maitra, F. M. Nogueira, E. Gross, and A. Rubio (Springer Berlin Heidelberg, Berlin, Heidelberg, 2012) pp. 167–184.
- ¹⁶⁷N. T. Maitra, *J. Chem. Phys.* **144**, 220901 (2016).
- ¹⁶⁸G. Strinati, *Phys. Rev. B* **29**, 5718 (1984).
- ¹⁶⁹M. Rohlfing and S. G. Louie, *Phys. Rev. B* **62**, 4927 (2000).
- ¹⁷⁰Y. Ma, M. Rohlfing, and C. Molteni, *Phys. Rev. B* **80**, 241405 (2009).
- ¹⁷¹Y. Ma, M. Rohlfing, and C. Molteni, *J. Chem. Theory Comput.* **6**, 257 (2009).
- ¹⁷²M. S. Kaczmarek, Y. Ma, and M. Rohlfing, *Phys. Rev. B* **81**, 115433 (2010).
- ¹⁷³B. Baumeier, D. Andrienko, and M. Rohlfing, *J. Chem. Theory Comput.* **8**, 2790 (2012).
- ¹⁷⁴B. Baumeier, D. Andrienko, Y. Ma, and M. Rohlfing, *J. Chem. Theory Comput.* **8**, 997 (2012).
- ¹⁷⁵M. Rohlfing, *Phys. Rev. Lett.* **108**, 087402 (2012).
- ¹⁷⁶T. Lettmann and M. Rohlfing, *J. Chem. Theory Comput.* **15**, 4547 (2019).
- ¹⁷⁷D. Bohm and D. Pines, *Phys. Rev.* **82**, 625 (1951).
- ¹⁷⁸D. Pines and D. Bohm, *Phys. Rev.* **85**, 338 (1952).
- ¹⁷⁹D. Bohm and D. Pines, *Phys. Rev.* **92**, 609 (1953).
- ¹⁸⁰X. Ren, P. Rinke, C. Joas, and M. Scheffler, *J. Mater. Sci.* **47**, 7447 (2012).
- ¹⁸¹G. P. Chen, V. K. Voora, M. M. Agee, S. G. Balasubramani, and F. Furche, *Ann. Rev. Phys. Chem.* **68**, 421 (2017).
- ¹⁸²A. I. Krylov, *Chem. Phys. Lett.* **338**, 375 (2001).
- ¹⁸³E. Monino and P.-F. Loos, *J. Chem. Theory Comput.* **17**, 2852 (2021).
- ¹⁸⁴D. Casanova and A. I. Krylov, *Phys. Chem. Chem. Phys.* **22**, 4326 (2020).
- ¹⁸⁵E. Monino, M. Boggio-Pasqua, A. Scemama, D. Jacquemin, and P.-F. Loos, *J. Phys. Chem. A* **126**, 4664 (2022).
- ¹⁸⁶S. J. Bintrim and T. C. Berkelbach, *J. Chem. Phys.* **154**, 041101 (2021).
- ¹⁸⁷M. F. Lange and T. C. Berkelbach, *J. Chem. Theory Comput.* **14**, 4224 (2018).
- ¹⁸⁸R. Quintero-Monsebaiz, E. Monino, A. Marie, and P.-F. Loos, *J. Chem. Phys.* **157**, 231102 (2022).

- ¹⁸⁹J. Tölle and G. Kin-Lic Chan, *J. Chem. Phys.* **158**, 124123 (2023).
- ¹⁹⁰S. J. Bintrim and T. C. Berkelbach, *J. Chem. Phys.* **156**, 044114 (2022).
- ¹⁹¹M. J. van Setten, F. Caruso, S. Sharifzadeh, X. Ren, M. Scheffler, F. Liu, J. Lischner, L. Lin, J. R. Deslippe, S. G. Louie, C. Yang, F. Weigend, J. B. Neaton, F. Evers, and P. Rinke, *J. Chem. Theory Comput.* **11**, 5665 (2015).
- ¹⁹²G. Riva, T. Audinet, M. Vladaj, P. Romaniello, and J. A. Berger, *SciPost Phys.* **12**, 093 (2022).
- ¹⁹³V. Rishi, A. Perera, and R. J. Bartlett, *J. Chem. Phys.* **153**, 234101 (2020).
- ¹⁹⁴R. D. Mattuck, *A guide to Feynman diagrams in the many-body problem*, 2nd ed., Dover books on physics and chemistry (Dover Publications, New York, 1992).
- ¹⁹⁵L. S. Cederbaum and W. Domcke, in *Adv. Chem. Phys.* (John Wiley & Sons, Inc., 1977) pp. 205–344.
- ¹⁹⁶J. Oddershede, P. Jørgensen, and D. L. Yeager, *Comp. Phys. Comm.* **2**, 33 (1984).
- ¹⁹⁷A. Szabo and N. S. Ostlund, *Modern quantum chemistry* (McGraw-Hill, New York, 1989).
- ¹⁹⁸J. Schirmer, *Phys. Rev. A* **26**, 2395 (1982).
- ¹⁹⁹J. Schirmer, L. S. Cederbaum, and O. Walter, *Phys. Rev. A* **28**, 1237 (1983).
- ²⁰⁰J. Schirmer and A. Barth, *Z. Phys. A* **317**, 267 (1984).
- ²⁰¹A. Dreuw and M. Wormit, *Wiley Interdiscip. Rev. Comput. Mol. Sci.* **5**, 82 (2015).
- ²⁰²M. Gell-Mann and K. A. Brueckner, *Phys. Rev.* **106**, 364 (1957).
- ²⁰³P. Nozières and D. Pines, *Phys. Rev.* **111**, 442 (1958).
- ²⁰⁴D. Foerster, P. Koval, and D. Sánchez-Portal, *J. Chem. Phys.* **135**, 074105 (2011).
- ²⁰⁵P. Liu, M. Kaltak, J. c. v. Klimeš, and G. Kresse, *Phys. Rev. B* **94**, 165109 (2016).
- ²⁰⁶A. Förster and L. Visscher, *Front. Chem.* **9**, 736591 (2021).
- ²⁰⁷I. Duchemin and X. Blase, *J. Chem. Phys.* **150**, 174120 (2019).
- ²⁰⁸I. Duchemin and X. Blase, *J. Chem. Theory Comput.* **16**, 1742 (2020).
- ²⁰⁹I. Duchemin and X. Blase, *J. Chem. Theory Comput.* **17**, 2383 (2021).
- ²¹⁰A. Dreuw and M. Head-Gordon, *Chem. Rev.* **105**, 4009 (2005).
- ²¹¹J. Schirmer, A. B. Trofimov, and G. Stelter, *J. Chem. Phys.* **109**, 4734 (1998).
- ²¹²P. Ring and P. Schuck, *The Nuclear Many-Body Problem* (Springer, 2004).
- ²¹³H. van Aggelen, Y. Yang, and W. Yang, *Phys. Rev. A* **88**, 030501 (2013).
- ²¹⁴D. Peng, S. N. Steinmann, H. van Aggelen, and W. Yang, *J. Chem. Phys.* **139**, 104112 (2013).
- ²¹⁵G. E. Scuseria, T. M. Henderson, and I. W. Bulik, *J. Chem. Phys.* **139**, 104113 (2013).
- ²¹⁶Y. Yang, H. van Aggelen, S. N. Steinmann, D. Peng, and W. Yang, *J. Chem. Phys.* **139**, 174110 (2013).
- ²¹⁷Y. Yang, H. van Aggelen, and W. Yang, *J. Chem. Phys.* **139**, 224105 (2013).
- ²¹⁸H. van Aggelen, Y. Yang, and W. Yang, *J. Chem. Phys.* **140**, 18A511 (2014).
- ²¹⁹Y. Yang, D. Peng, J. Lu, and W. Yang, *J. Chem. Phys.* **141**, 124104 (2014).
- ²²⁰X. Zhang and J. M. Herbert, *J. Chem. Phys.* **142**, 064109 (2015).
- ²²¹D. Zhang and W. Yang, *J. Chem. Phys.* **145**, 144105 (2016).
- ²²²C. Bannwarth, J. K. Yu, E. G. Hohenstein, and T. J. Martínez, *J. Chem. Phys.* **153**, 024110 (2020).
- ²²³E. Rebolini, *Range-Separated Density-Functional Theory for Molecular Excitation Energies*, Ph.D. thesis, Université Pierre et Marie Curie — Paris VI (2014).
- ²²⁴J. Schirmer and A. B. Trofimov, *J. Chem. Phys.* **120**, 11449 (2004).
- ²²⁵M. Wormit, D. R. Rehn, P. H. Harbach, J. Wenzel, C. M. Krauter, E. Epifanovsky, and A. Dreuw, *Mol. Phys.* **112**, 774 (2014).
- ²²⁶M. Wormit, *Development and Application of Reliable Methods for the Calculation of Excited States: From Light-Harvesting Complexes to Medium-Sized Molecules*, Ph.D. thesis, Frankfurt University (2009).
- ²²⁷S. Albrecht, L. Reining, R. Del Sole, and G. Onida, *Phys. Rev. Lett.* **80**, 4510 (1998).
- ²²⁸L. X. Benedict, E. L. Shirley, and R. B. Bohn, *Phys. Rev. Lett.* **80**, 4514 (1998).
- ²²⁹A. Marini and R. Del Sole, *Phys. Rev. Lett.* **91**, 176402 (2003).
- ²³⁰W. Hanke and L. J. Sham, *Phys. Rev. B* **21**, 4656 (1980).
- ²³¹S. Yamada, Y. Noguchi, K. Ishii, D. Hirose, O. Sugino, and K. Ohno, *Phys. Rev. B* **106**, 045113 (2022).
- ²³²M. Schreiber, M. R. Silva-Junior, S. P. A. Sauer, and W. Thiel, *J. Chem. Phys.* **128**, 134110 (2008).
- ²³³M. R. Silva-Junior, M. Schreiber, S. P. A. Sauer, and W. Thiel, *J. Chem. Phys.* **133**, 174318 (2010).
- ²³⁴M. R. Silva-Junior, S. P. Sauer, M. Schreiber, and W. Thiel, *Mol. Phys.* **108**, 453 (2010).
- ²³⁵M. R. Silva-Junior, M. Schreiber, S. P. A. Sauer, and W. Thiel, *J. Chem. Phys.* **133**, 174318 (2010).
- ²³⁶A. M. Lewis and T. C. Berkelbach, *J. Chem. Theory Comput.* **15**, 2925 (2019).
- ²³⁷P.-F. Loos, B. Pradines, A. Scemama, E. Giner, and J. Toulouse, *J. Chem. Theory Comput.* **16**, 1018 (2020).
- ²³⁸M. Head-Gordon, R. J. Rico, M. Oumi, and T. J. Lee, *Chem. Phys. Lett.* **219**, 21 (1994).
- ²³⁹M. Head-Gordon, D. Maurice, and M. Oumi, *Chem. Phys. Lett.* **246**, 114 (1995).
- ²⁴⁰A. Trofimov and J. Schirmer, *Chem. Phys.* **214**, 153 (1997).
- ²⁴¹O. Christiansen, H. Koch, and P. Jørgensen, *Chem. Phys. Lett.* **243**, 409 (1995).
- ²⁴²G. P. Purvis III and R. J. Bartlett, *J. Chem. Phys.* **76**, 1910 (1982).
- ²⁴³J. F. Stanton and R. J. Bartlett, *J. Chem. Phys.* **98**, 7029 (1993).
- ²⁴⁴P. F. Loos, “QuAcK: a software for emerging quantum electronic structure methods,” (2019), <https://github.com/pfloos/QuAcK>.
- ²⁴⁵J. Čížek and J. Paldus, *J. Chem. Phys.* **47**, 3976 (1967).
- ²⁴⁶P. F. Loos, A. Scemama, A. Blondel, Y. Garniron, M. Caffarel, and D. Jacquemin, *J. Chem. Theory Comput.* **14**, 4360 (2018).
- ²⁴⁷M. Véril, A. Scemama, M. Caffarel, F. Lipparini, M. Boggio-Pasqua, D. Jacquemin, and P.-F. Loos, *WIREs Comput. Mol. Sci.* **11**, e1517.
- ²⁴⁸A. Endo, M. Ogasawara, A. Takahashi, D. Yokoyama, Y. Kato, and C. Adachi, *Adv. Mater.* **21**, 4802 (2009).
- ²⁴⁹H. Uoyama, K. Goushi, K. Shizu, H. Nomura, and C. Adachi, *Nature* **492**, 234 (2012).
- ²⁵⁰M. A. Baldo, D. F. O'Brien, Y. You, A. Shoustikov, S. Sibley, M. E. Thompson, and S. R. Forrest, *Nature* **395**, 151 (1998).
- ²⁵¹C. Adachi, M. A. Baldo, M. E. Thompson, and S. R. Forrest, *J. Appl. Phys.* **90**, 5048 (2001).
- ²⁵²P. de Silva, *J. Phys. Chem. Lett.* **10**, 5674 (2019).
- ²⁵³J. Sanz-Rodrigo, G. Ricci, Y. Olivier, and J. C. Sancho-García, *J. Phys. Chem. A* **125**, 513 (2021).
- ²⁵⁴G. Ricci, E. San-Fabián, Y. Olivier, and J. C. Sancho-García, *ChemPhysChem* **22**, 553 (2021).
- ²⁵⁵Y. Olivier, B. Yurash, L. Muccioli, G. D’Avino, O. Mikhnenko, J. C. Sancho-García, C. Adachi, T.-Q. Nguyen, and D. Beljonne, *Phys. Rev. Mater.* **1**, 075602 (2017).
- ²⁵⁶Y. Olivier, J.-C. Sancho-García, L. Muccioli, G. D’Avino, and D. Beljonne, *J. Chem. Theory Comput.* **9**, 6149 (2018).
- ²⁵⁷J. C. Sancho-García, E. Brémond, G. Ricci, A. J. Pérez-Jiménez, Y. Olivier, and C. Adamo, *J. Chem. Phys.* **156**, 034105 (2022).
- ²⁵⁸K. Curtis, O. Adeyiga, O. Suleiman, and S. O. Odoh, *J. Chem. Phys.* **158**, 024116 (2023).
- ²⁵⁹A. B. Trofimov, G. Stelter, and J. Schirmer, *J. Chem. Phys.* **117**, 6402 (2002).
- ²⁶⁰P. H. P. Harbach, M. Wormit, and A. Dreuw, *J. Chem. Phys.* **141**, 064113 (2014).

²⁶¹O. Christiansen, H. Koch, and P. Jørgensen, *J. Chem. Phys.* **103**, 7429 (1995).

²⁶²H. Koch, O. Christiansen, P. Jørgensen, A. M. Sanchez de Merás, and T. Helgaker, *J. Chem. Phys.* **106**, 1808 (1997).

²⁶³P.-F. Loos and D. Jacquemin, *J. Phys. Chem. Lett.* **11**, 974 (2020).